Journal of Visualized Experiments

Microfluidic co-culture models for dissecting the immune response in in vitro tumor microenvironments

--Manuscript Draft--

Article Type:	Invited Methods Article - JoVE Produced Video
Manuscript Number:	JoVE61895R1
Full Title:	Microfluidic co-culture models for dissecting the immune response in in vitro tumor microenvironments
Corresponding Author:	Luca Businaro ITALY
Corresponding Author's Institution:	
Corresponding Author E-Mail:	luca.businaro@cnr.it
Order of Authors:	Adele De Ninno
	Francesca Romana Bertani
	Annamaria Gerardino
	Giovanna Schiavoni
	Martina Musella
	Claudia Galassi
	Fabrizio Mattei
	Antonella Sistigu
	Luca Businaro
Additional Information:	
Question	**Response**
Please indicate whether this article will be Standard Access or Open Access.	Standard Access (US$2,400)
Please indicate the **city, state/province, and country** where this article will be **filmed**. Please do not use abbreviations.	Rome, Italy
Please confirm that you have read and agree to the terms and conditions of the author license agreement that applies below:	I agree to the Author License Agreement
Please specify the section of the submitted manuscript.	Bioengineering
Please provide any comments to the journal here.	

TITLE:

Microfluidic Co-Culture Models for Dissecting the Immune Response in in vitro Tumor Microenvironments

AUTHORS AND AFFILIATIONS:

Adele De Ninno[1], Francesca Romana Bertani[1], Annamaria Gerardino[1], Giovanna Schiavoni[2], Martina Musella[3], Claudia Galassi[3], Fabrizio Mattei[2], Antonella Sistigu[3,4], Luca Businaro[1]

[1] CNR Institute for Photonics and Nanotechnology, Rome, Italy
[2] Dept. of Oncology and Molecular Medicine, Istituto Superiore di Sanità, Rome, Italy
[3]Istituto di Patologia Generale, Università Cattolica del Sacro Cuore, Rome, Italy
[4]Tumor Immunology and Immunotherapy Unit, IRCCS Regina Elena National Cancer Institute, Rome, Italy

adele.deninno@cnr.it
bertanifrancescaromana@gmail.com
annamaria.gerardino@cnr.it
giovanna.schiavoni@iss.it
martinamusella90@gmail.com
galassi.claudia@virgilio.it
fabrizio.mattei@iss.it
antonella.sistigu@gmail.com
luca.businaro@cnr.it

corresponding authors:

Adele De Ninno (adele.deninno@cnr.it), Antonella Sistigu (antonella.sistigu@gmail.com)

KEYWORDS

Organs-on-chip, tumor immunology, cancer-immune crosstalk, tumor microenvironment, immune contexture, cellular dynamics and interactions, microfluidic immuno-competent tumor-on-chip, immuno-oncology, cell tracking

SUMMARY

In the age of immunotherapy and single-cell genomic profiling, cancer biology requires novel in vitro and computational tools for investigating the tumor-immune interface in a proper spatiotemporal context. We describe protocols to exploit tumor-immune microfluidic co-cultures in 2D and 3D settings, compatible with dynamic, multiparametric monitoring of cellular functions.

ABSTRACT

Complex disease models demand cutting-edge tools able to deliver physiologically and pathologically relevant, actionable insights, and unveil otherwise invisible processes. Advanced cell assays closely mimicking in vivo scenery are establishing themselves as novel ways to visualize and measure the bidirectional tumor-host interplay influencing the progression of cancer. Here we describe two versatile protocols to recreate highly controllable 2D and 3D co-cultures in microdevices, mimicking the complexity of the tumor microenvironment (TME), under natural and therapy-induced immunosurveillance. In section

1, an experimental setting is provided to monitor crosstalk between adherent tumor cells and floating immune populations, by bright field time-lapse microscopy. As an applicative scenario, we analyze the effects of anti-cancer treatments, such as the so-called immunogenic cancer cell death inducers on the recruitment and activation of immune cells. In section 2, 3D tumor-immune microenvironments are assembled in a competitive layout. Differential immune infiltration is monitored by fluorescence snapshots up to 72 h, to evaluate combination therapeutic strategies. In both settings, image processing steps are illustrated to extract a plethora of immune cell parameters (e.g., immune cell migration and interaction, response to therapeutic agents). These simple and powerful methods can be further tailored to simulate the complexity of the TME encompassing the heterogeneity and plasticity of cancer, stromal and immune cells subtypes, as well as their reciprocal interactions as drivers of cancer evolution. The compliance of these rapidly evolving technologies with live-cell high-content imaging can lead to the generation of large informative datasets, bringing forth new challenges. Indeed, the triangle ''co-cultures/microscopy/advanced data analysis" sets the path towards a precise problem parametrization that may assist tailor-made therapeutic protocols. We expect that future integration of cancer-immune on-a-chip with artificial intelligence for high-throughput processing will synergize a large step forward in leveraging the capabilities as predictive and preclinical tools for precision and personalized oncology.

INTRODUCTION

The evolution of different branches of medicine as experimental disciplines has depended on the ability to manipulate cell population and organ functions under controlled conditions[1]. Such ability has its roots in the availability of measurable models able to recapitulate processes happening in our body.

In the age of immunotherapy and single-cell genomic profiling[2], cancer biology needs to take advantage of emerging in vitro and computational models for investigating the tumor-immune interface in a proper spatiotemporal context[2, 3].

The tumor microenvironment[4] (TME) is a complex tissue where cancer cells continuously interact and dynamically co-evolve with the other cellular (immune, stromal, and endothelial cells) and non-cellular (the extracellular matrix, ECM) components. The dynamic nature of this complex landscape dictates whether immune cells play as friends or foes of malignant cells, thus strongly affecting both disease progression and response to therapy. Nowadays, great efforts from onco-immunologists, bioinformaticians, and systems biology experts are converging to address the clinical significance of cancer heterogeneity[5,6], either in the space (i.e., in distinct tumoral regions) and time (i.e., at distinct tumor progression stages)[5,6], and to characterize cancer and immune cell phenotype and function at a single-cell level. As an example of this synergy, advanced computer-vision techniques are now routinely used for spatial mapping of immune infiltrate in histological samples[7,8].

On the front of experimental models, bridging animal studies and traditional in vitro methods, advances in microfluidics and co-culturing techniques give access to different classes of micro-engineered cellular models such as organoids, micro-physiological systems[9,10,11] (MPS), and organs-on-chip[12–14] (OOC). They share the common trait to zoom in the 'big picture' view of the cellular ecosystems and expanding the in vitro potential to control microenvironmental factors while exploiting high-content microscopy[15] and image processing approaches.

Nowadays, state-of-the-art- MPS and OOC systems have begun to include immunological aspects , incorporating different subtypes of immune cells in existing tissues- and co-cultures, so to explore and measure a variety of processes like inflammatory diseases, wound healing, mucosal immunity, and response to toxins or daily food products[16]. TME-on-a-chip models[10-17], also integrated with perfusable microvessels[18–21], have been developed to investigate cell-type-dependent interactions, physical and chemical perturbations, and the cytotoxic activity of infiltrating lymphocytes[22], as well as clinically relevant immunomodulatory agents[23].

Here, we provide versatile protocols, spanning from loading cells in chips to image processing tools, to exploit advanced tumor-immune microfluidic co-cultures in 2D (section 1) and 3D (section 2) settings[16], compatible with dynamic, multiparametric[24] monitoring and visualization of cellular functions. This is achieved maintaining easiness of use and flexibility both in sample management and data analysis, taking advantage of Fiji freeware software and its toolboxes[25,26].

The microfluidic device, described in section 1, is designed to perform 2D co-cultures of adherent cancer and floating immune cells. This platform was validated for the in vitro measurement of immune cell behavior in the presence of genetic mutations[27] and/or immunodeficiencies[28]. Here, we illustrate steps for tracking immune cells in time-lapse bright-field images, by exploiting a semi-automatic method based on Trackmate (a plugin implemented in Fiji software). This procedure enables the extraction of kinematic descriptors of immune migration [29] and response (i.e., interaction times) to target cancer cells, treated or not with immunogenic cell death inducers[27].

Importantly these parameters, extracted from time-series images, can be processed with advanced mathematical machinery. As an example of the potentiality of this approach, our groups recently published an analysis based on mathematical methods from stochastic processes and statistical mechanics to model cellular network properties and provide a parametrized description of immune cell behavior (i.e., biased or uncorrelated random walk, highly or not coordinated motion[30,31]).

The 3D setting, provided in the second section, is based on a co-culture protocol to recreate more complex immunocompetent TMEs embedded in two gel regions with different combinations of cell types and drugs in a competitive fashion. Here, image processing steps are described to measure, at different timepoints, the infiltration of stained immune cells in human A375M melanoma cells cultivated within Matrigel, to evaluate antitumor agent combinations[32]. A375M line, an A375P derived cell line characterized by a highly metastatic phenotype was chosen to evaluate their metastatic capability in the presence of immune cells[32].

The described models can be fully compliant with different cell sources (murine and human immortalized or primary cell lines, organoids, xenografts, among the others). In recent studies of our lab, by combining high-content video microscopy with image analysis, the competitive 3D layout was applied to investigate: i) an anti-tumoral (antibody-dependent cell-mediated cytotoxicity, ADCC) immune response and dissect the role of fibroblasts in resistance to trastuzumab therapy in $HER2^{+}$ breast cancer on-chip models[33]; ii) the action of myeloid cells

(i.e., cancer-associated macrophages) in mechanisms of tumor evasion and recruitment of T cells[34]; iii) the efficacy of immunotherapeutic regimes, specifically based on Interferon-α-conditioned dendritic cells (IFN-DCs), cultivated with drug-treated colon cancer cells in collagen matrices, and to evaluate efficient motion and the succeeding phagocytosis events[35]; iv) the chemotactic migration of bone marrow-derived eosinophils towards IL-33 treated or untreated melanoma cells[36].

These advanced models could serve as observation windows for understanding the role of immune contexture in cancer metastasis and resistance mechanisms, but efforts are required to translate findings into the clinics, closing the gap with basic research[37].

As an emerging scenario, harnessing the power of automated high-content microscopy coupled to the use of more physiologically-relevant microsystems is opening novel potential challenges for the handling, processing, and interpretation of hundreds, and even thousands, of Gigabytes of multiparametric data, which can be generated from a single experimental campaign. This implies a direct link of OOC experiments with artificial intelligence[38,39, 40,41,42] (AI)-based algorithms both for advanced automated analysis, and generation of features which can feed in turn in silico models of cancer-immune interplay[43], with exciting new applications at the horizon, such as the development of predictive drug screening assays[44].

An ever-expanding flow of efforts is focused on the design of disease models jointly with the optimization of strategies to implement the large-scale perturbation screens with single-cell multi-omics readouts. This will undoubtedly help the development and, hopefully, the clinical implementation, accompanied by an appropriate degree of method standardization, of a systematic onco-immunology-on-a-chip approach to gain novel insights into immune disorders and cancer dissemination mechanisms.

PROTOCOLS

1. Chip design for adherent and floating cells 2D co-cultures

NOTE: The 2D co-culture layout (**Figure 1A-C**) is characterized by three chambers (100 µm high) interconnected by two sets of microchannel arrays (500 x 12 x 10 μm^3, L×W×H). The intermediate chamber forms two closed dead-end compartments which block floating immune cells overflowing into the tumor site during the loading step 1.2.5. This device type is useful for real-time bidimensional measurements of single-cell (either adherent or floating) motility, and of cell-cell interactions[16,27,28,30,31]. A typical cell migration study (conducted from several hours to several days) combines live-cell microscopy with image-processing algorithms[45], in order to translate the acquired image sequences into numerical features[25]. Based on the migratory patterns, several biophysical indicators can be estimated, such as the displacement and velocity of cells, as well as the duration of immune cell and target cell interactions[24,46].

1.1. Preparation of cancer and PBMC cells

1.1.1. Cancer cell culture

NOTE: MDA-MB-231 triple-negative [estrogen receptor (ER)-, progesterone receptor (PR)-, and human epidermal growth factor receptor 2 (HER2)-] human breast adenocarcinoma cells are routinely grown in a Roswell Park Memorial Institute (RPMI) 1640 medium supplemented with 10% (v/v) fetal bovine serum (FBS), 2 mM L-glutamine, 100 IU mL^{-1} penicillin G sodium salt and 100 µg mL^{-1} streptomycin sulfate (growth medium), under standard culture conditions (37 °C and 5% CO_2).

1.1.1.1. To optimize cell culture growth, plate MDA-MB-231 cells in 75 cm^2 flasks at a density of 1×10^6 cells mL^{-1} in 12-to-15 mL of growth medium.

1.1.1.2. When cells reach the 75-80% of confluence, discard the growth medium, wash cells with pre-warmed phosphate-buffered saline (PBS) to completely remove FBS, and then detach them with pre-warmed trypsin (1-to-2 min at 37 °C).

1.1.1.3. Add growth medium to inactivate trypsin enzymatic activity and collect detached cells. Wash cells twice for 5 min at 1,100 x *g* at room temperature (RT).

1.1.1.4. Count cells in a cell counting slide by means of Trypan Blue dye exclusion test and then reseed them either for maintenance culture (for no more than 6 passages from thawing) or for experimental procedures.

1.1.1.5. For microfluidic experiments, seed 1×10^6 cells in 6-well plates in 3 mL of growth medium and either treat with 25 µM doxorubicin (DOXO) or an equal volume of DOXO solvent (PBS) as control.

1.1.1.6. Four-to-6 hours after, wash DOXO-treated cells twice with pre-warmed PBS for 5 min at 1,100 x *g* at RT.

1.1.1.7. Count DOXO-treated and PBS-treated control cells as above (see step 1.1.1.5) and set the co-culture with peripheral blood mononuclear cells (PBMCs) in microfluidic devices.

1.1.2. PBMC isolation

1.2.1 Collect venous whole blood (10 mL approximately) from healthy volunteers in heparinized vials and gently mix by inverting the tube 2-to-4 times[47].

1.2.2 Dilute blood 1:1 with PBS and layer over 10 mL of density gradient medium Lymphoprep in a 50 mL tube.

NOTE: Ensure to do the layering very gently and slowly to let blood and Lymphoprep form two distinct layers.

1.2.3 Centrifuge tubes for 30 minutes at 400 x *g* at 4 °C in a swing-out bucket without brakes. Four distinct layers will form: (i) plasma at the top, (ii) a white and cloudy layer containing PBMCs, (iii) Lymphoprep, and (iv) a pellet of erythrocytes and granulocytes.

1.2.4 Aspirate gently PBMCs with a 2 mL pipette and immediately resuspend in warm growth medium (same used in step 1.1.1) and wash twice for 5 min at 1,100 x *g* at RT.

1.2.5 Count pelleted PBMCs as above (see step 1.1.1.5) and either use for experimental procedures or freeze for long-term storage.

1.2. Plating the cells in 2D chips

NOTE: PBMCs are not stained in this protocol. To characterize specific phenotypes on-chip, immune cell sub-populations can be isolated by immunomagnetic bead selection, stained with fluorescent cell trackers, re-mixed with the unlabeled remaining fraction, and thus confronted with target cancer cells, as reported in the on-chip experiments, described in Vacchelli et al.[27], and in Racioppi et al.[34].

1.2.1. Before starting co-culture experiments and to facilitate the addition of reagents, activate stored chips by an oxygen plasma treatment for a few seconds. Immediately fill reservoirs with deionized water or PBS to keep PDMS (polydimethylsiloxane) surfaces hydrophilic until plating steps.

NOTE: PDMS is intrinsically hydrophobic, which may result in difficulties in operating and in the entrapment of air bubbles in microchannels. See step 7 in the supplementary file providing details about oxygen plasma activation.

1.2.2. Sterilize under a UV cabinet for 20 min, wash 2-3 times with fresh PBS, and then incubate with culture media for 1 h. Keep chips in incubator until performing plating steps.

1.2.3. Withdraw excess media from all six reservoirs. Take care to avoid sucking up media from the main culture chambers.

1.2.4. Slowly apply 1×10^5 cells resuspended in 10-20 µL of growth medium in the upper left-hand reservoir, and then in the lower well (**Figure 1A**, reservoirs 1 and 2). Wait 5 min to let cells adhere into the tumor chamber. Some cells will settle and attach in the reservoirs.

NOTE: Insert cellular suspension next to the channel openings. This procedure is applied to MDA-MB-231 cancer cells, other lines will require cell density optimization. To improve cancer cell attachment, a coating functionalization of surfaces (e.g., poly-L-lysine, fibronectin) can be performed. Please, refer to previously published protocols for coating steps[16, 48–50].

1.2.5. On the right side gently pipet 1×10^6 PBMC resuspended in 50 µL of growth medium into wells 3 and 4 (see **Figure 1A**, reservoirs 3 and 4).

NOTE: After flowing, PBMC will distribute into the intermediate chamber creating a “front”, which represents the starting point of the experiment.

1.2.6. Fill all the six reservoirs with up to 100-150 µL of growth medium. Under a microscope check that cells have distributed correctly in the culture compartments as

depicted in **Figure 1D-E**. Final volumes can vary with the size of the reservoirs. Adjust volumes to be equal in all wells.

1.2.7. Place the chips back in the incubator for approximately 1 h to stabilize the system prior to time-lapse recording. Add fresh medium every 3 days, as it may be subjected to evaporation losses.

NOTE: The system is compatible with both live/dead-cell analysis and dynamic multiplex cytokine secretion profiling from conditioned media. For chemokine analyses, up to 200-250 µL aliquots of supernatants may be accessible by collecting media from the two reservoirs of each compartment. Classical ELISA and Luminex cytokine profiling assays require about 50 µL of supernatants. Please see [51, 52] examples of studies of other labs performing cytokine profiling on OOC models.

1.3. Time-lapse acquisition of unlabeled cancer and immune cells

NOTE: Typically, 3 chips are arranged on a single microscope slide (see **Figure 1A** for 2D chip and **Figure 4A** for 3D chip). Using stage holders allocating 4 slides, co-cultures can be suitable to be monitored by automated high-content microscopy to analyze large batches of experimental conditions. Chips can be easily mounted on slides with thickness equal to 1 mm or 170 microns (plastic or glass coverslips, 6-well optical bottom multi-wells) for high-resolution confocal imaging.

1.3.1. Record bright-field image series of unlabelled cells by means of a video microscopy setup equipped with an incubation system.

NOTE: Here time-series datasets (time window: 48 h, frame rate: 2 min) were acquired with a fluorescence microscope, equipped with a 4x objective and CMOS 1.3M pixels, optimized to fit into a standard cell culture incubator.

1.3.2. Warm up the microscope for at least 2 h to equilibrate to 37 °C and 5% CO_2 before starting acquisition.

1.3.3. Select the window of observation by centering the microchannel array between the tumor and the central compartment. This allows to visualize the dynamics of immune infiltration and the interactions within the region in which cancer cells are seeded.

1.3.4. Adjust the illumination intensity and focus of cancer and immune cells.

1.3.5. For launching time-lapse acquisition, optimize frame rate and time duration according to experiment and cell type under study.

NOTE: Imaging conditions must be optimized to avoid excessive photo-exposure while maintaining a good signal-to-noise ratio (SNR). As immune cells are very motile, the acquisition frame rate needs to be sufficiently high to follow the dynamic process of interest and enable easy tracking[53]. A compromise should be reached between the tracking algorithm, the compatibility with the size of the resulting dataset, and the viability, density,

and motility of observed cells.

1.3.6. At the end of the time-lapse, use the function **Import Image Sequence** and **Save as** of the ImageJ software to convert the frame dataset in a 25 fps uncompressed video file.

NOTE: The generated video file is now ready for cell tracking analysis. Here, RGB (1280x1024 pixels) images were collected with a spatial resolution of 1.33 µm/pixel. A 24 h duration movie (3.5 GB stack) of a single field of view (FOV) consists of 720 frames for each condition.

1.4. Data analysis: Semi-automatic extraction of unlabeled immune tracks by Trackmate

NOTE: Here, immune motility analysis in 2D unlabeled time-lapse images is carried on using TrackMate[54], an open-source toolbox available in the Fiji/ImageJ software bundle (https://imagej.nih.gov/ij/). Several algorithms are provided to perform automated single-particle tracking[55] (SPT) of spot-like structures. They have been applied efficiently to fluorescent images, where objects are bright over a dark background with high SNR (i.e., sub-resolution fluorescent spots, labeled traffic vesicles, nuclei)[1, 25, 56–58]. SPT is mainly based on two sequential steps. First, objects are localized with identified positions in multiple frames (segmentation), as schematized in **Figure 2**. In the second stage (particle linking), detected spots are linked over consecutive frames to estimate motion and reconstruct their trajectories, in the shape of a track (**Figure 3**). Numerical features can be computed from each extracted X, Y, Z coordinates array over time. Extended documentation is reported in [54] as well as online (https://imagej.net/TrackMate), following the Getting started with TrackMate tutorial. The accuracy of the process can be inspected immediately, handling an intuitive graphical user interface (wizard-like GUI) that enables users, at every step, to readjust settings. The following part briefly depicts how to use Trackmate for image processing and quantification steps, applied to visible light images:

1.4.1. Drag and drop the full-time video/image stack on the Fiji toolbar.

1.4.2. Calibration stack setup (**Figure 2A**).

1.4.2.1. Check the dimensionality and assign the image properties by selecting **Image> Properties**. Fill **Unit of length**, **Pixel dimensions** and **Frame interval** boxes.

1.4.2.2. To perform the calibration, use the known length of the microchannels (500 µm, **Figure 1C**) and divide by the corresponding measured length in pixels. For 2D time-series, make sure to swap Z/T field entering 1 as z-slice and the correct number of movie frames. If not accomplished, Trackmate quantitative outputs and parameters will be reported in pixel units and timeframes.

1.4.3. Pre-processing of images

1.4.3.1. To enhance the correct discrimination of immune cells from a noisy background, pre-process bright-field images to compensate artifacts. Ensure that datasets consist of 8-bit TIFF images (brightness range: 0–255).

NOTE: Uneven illumination, low SNR, and contamination by small debris particle in visible light images could compromise the success of a cell tracking process. Here, time-series datasets are pre-processed through background subtraction, brightness/contrast adjust function, and by local image subtraction of a Gaussian blur from original images. There are other different analysis toolkits available in ImageJ for processing and segmentation of phase-contrast or bright-field images, including Empirical Gradient Threshold (EGT)[59].

1.4.4. First calibration panel (**Figure 2A**)

1.4.4.1. Revise/confirm the dimensionality and temporal window of data (i.e., pixel-width and frame interval).

NOTE: TrackMate automatically reads in the image properties box to give the final tracking results in calibrated physical units (i.e., µm and minutes).

1.4.4.2. Define a region of interest to compute the extraction of immune tracks, by manually inserting values or by drawing a closed area over the active image and then press the Refresh source button. To extract global immune migration paths, select rectangular regions respectively on the right side of microchannels (central chamber, **Figure 1F**) and on the left (tumor chamber, **Figure 1E**).

1.4.4.3. To analyze interactions between cancer and immune hotspots, draw circular sub-regions by using ROI tools (go to **Edit → Selection → Specify**).

NOTE: When running for the first time this toolbox on a new biological application, spend the necessary time to optimize settings for reconstructing the tracks.

1.4.4.4. Perform manual tracking of the cell trajectories (about 50-100 cells) to find empirically the right configuration and next to validate as a benchmark the reliability of automatic extraction of movements. Additionally, work initially on a smaller area to easily check the accuracy of the chosen parameters.

1.4.5. Immune spots detection step (**Figure 2B**)

1.4.5.1. Select the default **Laplacian of Gaussian** (LoG) detector. The LoG detector works to find bright, blob-like, roundish objects and applying a Laplacian of Gaussian filter on the image tuned for intermediate spot sizes (5-to-20 pixels in diameter).

1.4.5.2. In **Estimated Blob Diameter** (here, 10–13 µm) enter a value slightly bigger than the expected spot size. Increase **Threshold** (here 1-3 µm) value until extra spurious background spots are reduced possibly without removing the object features. Detections below **Threshold value** (based on a quality metrics) will be discarded from subsequent analysis. Check the box for the median filter and sub-pixel localization to improve the quality of spot detection.

1.4.5.3. Use the **Preview** button to view and quickly inspect identified immune cells overlaid on the images by magenta-colored circles. Mistakes during the detection will have a

considerable impact on the linking process. Other unwanted detections can be corrected in the subsequent menus by user-defined filters (i.e., by spot intensity, size, or position).

1.4.6. Once satisfied with selections, hit **Next**. These settings may vary depending on experimental and acquisition imaging modalities (e.g., FOV, objective magnification, bright-field or fluorescent images) setup, cell type (adherent or floating cells), from slow or fast motility, kind of cellular behavior (interacting or not) and low/medium/high density in the observation area.

1.4.7. Proceed and skip **Initial Thresholding** menu. Select the **Hyperstack Displayer** window.

1.4.8. **Filter on spots''** panel (**Figure 2C**).

1.4.8.1. Select: **Uniform Color**. Filters, as shown in **Figure 2C**, can be added to retain labeled spots with feature values, displayed in a histogram, above or below a reversible threshold.

1.4.8.2. Tracker selection stage (**Figure 3A**). Choose the **Simple LAP tracker**, as particle linking algorithm asking for three fields to fill (in this case, "Linking max distance": 30-50 µm, "Gap-closing max distance": 25-50 µm, "Gap-closing max frame gap": 4-6). This detector manages gap-closing events, with cost linking calculation solely based on their respective distance.

NOTE: The maximal allowed linking distance limits the spatial search range for candidate matching spots, corresponding to the maximally allowed displacement traveled by between two subsequent frames (**Figure 3D**).

1.4.8.3. Provide larger values of maximal displacement when the fragmentation of tracks of highly motile particles is noticed. Two-track links will not be connected if the frame-to-frame movement is larger than the given maximal distance value. If segments bridge badly two different cells, decrease the value of maximal displacement.

1.4.8.4. Try to reconnect missing spots, varying the values of "the max distance for gap closing" and "the maximal frame gap". These parameters deal with gap-closing events in non-adjacent frames. Spot disappearance may occur for some frames (i.e., out of focus particles, cells leaving out and in the FOV, segmentation failures in a noisy image).

NOTE: To handle splitting or merging events, opt for LAP linker as detector which introduces linking cost matrix penalties.

1.4.9. Click **Next** to run the tracking computation. Press **Next**.

1.4.10. **Filtering tracks** panel (**Figure 3B**). Change the color of immune paths selecting, from the drop-down menu, "**Track ID**" or other track features. At this point, choose optionally to set interactive filters functional, to improve the quality of the outcome and revisit the procedure.

NOTE: Spurious spots arise from noise in the image and loss of feature quality. This will generate short segments while cells of interest can be tracked over many frames.

1.4.11. As a strategy try to filter out, based on the number of spots they contain. Additionally, sort tracks using a combination of options such as **Track displacement**, **Track duration** or **Minimal/Mean/Maximal Velocity** to exclude false or unwanted tracks (with fewer frames respect to overall duration of time-lapse or involving dirty or not moving particles) from further post-processing.

NOTE: The choice of filters can vary depending on the specific application and biological system.

1.4.12. Examine all tracks in the **Display Options** interface, scroll through time, and verify how accurate tracks match cell migration paths. The drop-down menu provides color codes for spots and paths for easy visualization and filtering by several modalities (e.g., kinetic parameters, intensity, temporal or spatial position).

NOTE: For tracking high-density cultures, or high-motile cells, increase the acquisition frame rate minimizing cell displacement traveled in consecutive time intervals.

1.4.13. Manual correction of segmentation and linking mistakes (**Figure 3E**).

1.4.13.1. To enhance further the quality of results, edit manually spots (debris particles, stationary cells) and remove erroneous tracks deriving from detected tumor boundaries when analyzing tumor-immune interaction ROIs.

1.4.13.2. First, select the TrackMate tool in the ImageJ toolbar. For eliminating an existing spot throughout the whole stack, press shift and create by mouse cursor a ROI mask over the target spot (edited in a green circle), and then hit the DEL key.

1.4.13.3. For adding a new spot (in case of missing tracks due to spots disappearance) press the A key, laying the mouse at the pointed location. Repeat the tracks-linking computation process after this step.

1.4.14. When satisfied, select **Analysis** in the **Display Options** panel to generate three text files (**Figure 3C**). The table in “Spots in tracks statistics” provides the spatiotemporal coordinates of immune spots (X-Y-Z positions of the cells labeled with the associated frame and track number). “Links in tracks statistics” and “Track statistics” contain information relative to the tracks: track durations, number of detected gaps or spots, track initial and stop-frame, etc. Save and export for each dataset.

NOTE: When clicking on a row within the result windows, the respective spot, link, or track is activated within the time-lapse video for visual inspection. Repeat the filtering steps to select/remove tracks. All future exported data will be updated. TIP: Track initial and stop-frame and track duration values can be exploited to calculate times of contact between cancer and immune cells when processing ROIs of interaction.

1.4.15. Press the **Save** button to generate a resulting XML file containing all the parameter values, the path to images, and spot positions in time. The ''Load TrackMate file'' command restores the whole process session for each movie file individually.

1.4.16. Move to the last panel of the GUI called **Select an action**. In the list, use **Capture overlay > Execute** function to produce a video with tracks overlaid. TIP: "N-spots *vs* time" option may be used to compute the spatial density of immune cells in a ROI (**Figure 6B**, right panel).

1.4.17. Post-processing analysis and migration statistics

1.4.17.1. Analyze the raw positional data directly in Trackmate or export data to calculate comprehensive kinetic parameters[29] (i.e., total trajectory length, Euclidean distance, confinement ratio, mean-squared displacement[56], average or instantaneous track velocity, arrest coefficient, distribution of angles of migration, Forward migration index, mean straight-line speed) to classify immune cell migration behavior (e.g., directed or diffusive motion[30, 31]) and response to target cancer cells (e.g., treated *vs* control).

NOTE: Additional useful plugins such as The Chemotaxis and Migration Tool (http://ibidi.com/software/chemotaxis_and_migration_tool/) provides various graphs (e.g., Rose or sector plots, such as depicted in **Figure 6**) and statistical tests for advanced analysis and visualization of experimental migration and chemotaxis data. Combining cell tracking and cell segmentation algorithms[24, 25, 45] may enable measurements of morphological metrics at the single-cell level (i.e., cell surface area, the major and minor axis length, and the cell aspect ratio).

2. 3D immuno-competent cancer on-chip model in a competitive assay

NOTE: The 3D chip design, depicted in **Figure 4**, consists of 5 major compartments: a central one for the floating immune cells intake, two side regions for embedding tumor cells in hydrogel matrices (150-250 µm high), and media perfusion chambers. Immune and tumor chambers are connected by two sets of narrow arrays of microchannels (200×12×10 μm^3, L×W×H, **Figure 4E**). Regularly 100 µm-spaced trapezoidal isosceles micropillars (about 25-30 interfaces for each side gel region, **Figure 4C**) work as barriers to confine gel solution during injection exploiting the balance between surface tension and capillary forces[60, 61] and connect tumor regions to the two lateral additional media chambers in order to set a gel-liquid interface (**Figure 5**). The detailed features of the 3D competitive assay are shown in **Figure 4**. Preferential migration of immune cells towards the two hydrogel compartments hosting tumoral cells that have undergone different treatments can be monitored and quantified. The particular competitive layout can be applied to investigate a plethora of different cancer biology phenotypes (e.g., drug-resistant vs aggressive, primary or metastatic, responders vs non-responders). Additionally, the gel embedded regions can be easily integrated with different cell populations to recreate more heterogenous TMEs, including stromal components (fibroblasts, endothelial cells)[23] or to simulate specific immunosuppressive milieu[34] (e.g., macrophages) for dissecting mechanisms of drug resistance and tumor evasion.

NOTE: Nuclear and active caspase staining, by using commercial kits for Live/dead assays (e.g., Thermo Fisher Scientific, Incucyte reagents), can be implemented to assess mitotic or apoptotic death events, as reported in Nguyen et al.[33].

2.1. Preparation of matrix solution with cells and Loading in the device

NOTE: In the following experimental setting, the two gel regions contain mixtures of human A375M melanoma cell lines, grown in matrix solution (e.g., Matrigel), exposed to therapeutic agents used as monotherapy or in combination. This setting allowed us to evaluate the efficacy of a combination of two drugs with respect to single ones in a competitive fashion and to quantify their ability to attract PBMCs.

2.1.1. Defrost a stock of matrix solution (e.g., Matrigel) by placing on ice into a 4 °C refrigerator one day before the experiment.

NOTE: Do not expose the product to multiple freeze-thaw cycles as it becomes "clumpy". Other synthetic or natural hydrogels protocols can be suitable to be used in this setting. Please refer to [33–35] for the preparation of cancer cells in collagen matrices.

2.1.2. Resuspend A375 human melanoma cells, stained with live-compatible PKH67 Green Fluorescent Cell Linker in matrix solution (2 mg mL^{-1}). Where indicated, add 5-aza-2'-deoxycytidine (DAC; 2.5 µM), referred as DAC, and/or IFN-α2b ,referred as IFN, at the proper doses[32].

NOTE: Match the Lot # on the bottle spec sheet. Based on the concentration calculate the volume of medium needed to make up to 2 mg mL^{-1} Please adjust the optimal protein concentration and cancer cell suspension concentration accordingly to your application of interest.

2.1.3. Pipette up and down carefully to avoid the generation of bubbles. Keep the microcentrifuge tube on ice while mixing to prevent any unwanted polymerization.

2.1.4. After sterilization, place the devices on ice (using an ice bucket and lid) to avoid matrix solution solidification during the whole procedure of cell loading.

2.1.5. Slowly inject the two IFN and DAC/IFN Matrigel/tumor cell mixtures (2-4 µL) into the left and right gel port, respectively with 10-µL micropipette using cold tips (**Figure 5A**). Apply gentle pressure to push matrix solution from one side until reaches the opposite one.

NOTE: The volume of matrix solution was chosen to avoid overflowing into adjacent channels. Do not exert excessive pipetting pressure to prevent the solution from leaking into the media and central channels. If during loading gel path is blocked along the channel, try to insert the solution from the other inlet until the gel fronts meet. When removing the micropipette from the inlets, hold the plunger, otherwise the negative pressure will aspirate matrix solution.

2.1.6. Place the device in an incubator in upright position at 37 °C and 5% CO_2 for 30 minutes to allow gelation of the matrix solution to take place (**Figure 5B**). Handle with care chips with

embedded unpolymerized gel to prevent leaking out of the gel channel.

2.1.7. In the meantime, resuspend PKH67-labelled PBMCs ($1x10^6$ cells) in 10 µL of complete DMEM (Dulbecco's modified Eagle's medium).

2.1.8. After matrix gelation, fill media channels with (50-100 µL) the same aliquot of culture medium in all six reservoirs to prevent gel drying in the chips. Keep in incubator until immune cell suspension seeding.

NOTE: Check under a microscope the correct and homogeneous distribution of tumor cells in the gel and the integrity of the polymerized gel barriers. Partially or not uniform gelled regions or bubbles in the mixture lead to the premature flowing of PBMCs in gel media channels at the starting point of the experiment due to pressure initial fluctuations.

2.1.9. Aspirate media from the six wells and position the tip near the inlet of a media channel to inject gently with moderate pressure PBMC cell suspension. The loading temporal sequence is depicted in **Figure 5C**:

1. PBMCs in 10 µL medium into the upper central well.
2. 50-100 µL medium into each of four wells of lateral channels.
3. 40-90 µL medium into the upper central well.
4. 50-100 µL medium into the lower central well.

2.1.10. Ensure under a microscope that the PBMCs distribution remains confined in the central chamber after the loading step. (**Figure 7A**).

NOTE: If it is not optimal, adjust the concentration if needed and repeat the seeding steps, using pristine chips. When calculating volumes for the planned experimental conditions, refer to an excess number of chips (15-20%) to take in account of potential errors and adjustments. Volumes and concentrations should be optimized according to the specific application.

2.1.11. Place assembled devices on a level surface in the incubator at 37 °C and 5% CO_2 for subsequent fluorescence imaging acquisition. Handle with care chips after loading immune cells which are floating.

NOTE: Compensate evaporative losses of volumes in reservoirs by replacing media every 2-3 days. For chemokine profiling, up to 100 µL from each of two wells of culture compartments can be aspirated, please refer to step 1.2.7, in step 1.

2.2. Automated Counting of recruited PBMCs in single-channel fluorescent images in ImageJ

NOTE: Classical methods of immunofluorescence for confocal high-resolution imaging can be applied to on-chip operations as endpoint measurements. The basic staining procedure involves cell on-chip fixation, permeabilization, blocking, antibody binding, staining of nuclei with washing steps in between. Unlabeled immune cells infiltrated in 3D gels regions with embedded cancer microenvironments can be fixed at desired time-points and stained for expression markers of activation/exhaustion /maturation (e.g., for CD8 cells, monitoring of

CD69, CD95, PD1, TIM3 markers). In Parlato et al.[35], phagocytosis of SW620 apoptotic cells was evaluated by confocal microscopy, using devices mounted on 170 µm-thick coverslips. IFN-DCs were stained adding on-chip anti-human HLA-DR-FITC Ab aliquots.

To calculate the extent of infiltrated fluorescently stained live immune cells challenged with competitive signals, a common image analysis workflow is set as follows (**Figure 7 D-G**):

2.2.1. Acquire, at specific time endpoints, phase contrast, and red/green channels fluorescence microphotographs of the left and right gel regions containing tumor cells respectively exposed to single or combinations of pharmacological regimes.

NOTE: Here images were captured by an EVOS-FL fluorescence microscope after cell loading (0 h), after 48 h and after 72 h of incubation (**Figure 7A-B**). A 4x-10x magnification was used to acquire the central chamber, the microchannel arrays, and the two juxtaposed side channels containing A375 plus IFN and A375 plus DAC/IFN.

2.2.1.1. When performing acquisition operations, consider the parameters to measure and avoid saturation of features to be counted. Optimal segmentation results depend on the nature of the acquired images, due to variability in the biological samples themselves, quality of staining, and the microscopy techniques utilized for user-oriented applications.

2.2.2. Load fluorescence single-channel data (in this case red = PBMCs), in Fiji by dragging it into the main window (**Figure 7D**). Duplicate the image to avoid overwriting the raw data during the selection of pre-processing filters until final segmentation.

2.2.2.1. If the image is a color image (RGB), hit **Image** > Type 8 or 16-bit to convert to greyscale. Check that Edit Options Conversions is set to **scale when converting**.

2.2.3. Preprocessing raw data via cleaning-up of noise and artifacts.

2.2.3.1. Go to **Process** > **Subtract Background** menu by applying the rolling ball algorithm to correct uneven noise background with large spatial variations of intensities. Set the radius to at least the size of the largest foreground particle.

2.2.3.2. Pick the **Preview** box for trial and error procedure to yield optimal results. Too small values may incorrectly remove structures of interest. In **Brightness&Contrast** command drag **Minimum/Maximum** sliders to change the range of intensities in the histogram. Shift the **Maximum** slider to the left to increase the brightness, without wash-out features. Move the **Minimum** slide to the right to increase the contrast of the image avoiding disappearance of less visible features in the background. Click **Apply** to fix changes.

2.2.4. Image Enhancement.

2.2.4.1. Go to **Process > Filters** and experiment with the Median, Gaussian filters on images (**Figure 7E**).

NOTE: Pre-filtering radius should be adapted to the image noise pixels. The non-linear Median

filter replaces pixel value with the median value of neighbours, to reduce salt-and-pepper noise. “Gaussian Blur” is used to smooth a digital picture, by replacing pixels with a weighted average of surrounding pixels. The weights come from the Gaussian probability distribution, so the nearest pixels are more influential.

2.2.4.2. Go optionally to **Process > Math > Gamma** with ticked **Preview** box to increase the contrast.

NOTE: Intensities set in the B&C panel are scaled between the two min and max limits. Values < 1.0 accentuate differences between low intensities while values > 1.0 accentuate differences between high intensities. Gamma correction is functional to find a display range, showing the dimmest objects without saturating the brightest.

2.2.5. Creation of a binary image mask.

2.2.5.1. Go to **Image > Adjust > Threshold**. The most simply employed method to determine thresholds relies on histogram analysis of intensity levels, as shown in **Figure 7F**. In the drop-menu, play with different global thresholding methods (in our case, Otsu is applied).

2.2.5.2. Manually scroll or type a known range of pixel intensities in the histogram panels, observe the change of the red pattern overlaying the image which mostly resembles the actual cell area. The **Reset** button removes the overlay. Once satisfied, click **Apply** to generate a binary version of the image. Check **Process** > **Binary > Options** to control how thresholded images are displayed and how objects are identified by the Particle Analyzer.

2.2.6. Use the menu command **Process/Binary/Watershed Particles** to divide partially overlapping or merged during the threshold. Watershed can often accurately cut them apart by adding a 1-pixel thick line. Perform morphological operations such as Dilate or Erode operations to either grow or remove pixels from under or over- saturated pixels.

NOTE: For more information *see* the Menu Commands section or refer to *MorphoLib*J, an integrated library based on mathematical morphology to process binary data.

2.2.7. Quantitative Image Feature Description.

2.2.7.1. Once obtained satisfactory object recognition, open the Particle Analyzer from **Analyze > Analyze Particles**. Particles can be excluded by their size and circularity, expressed in pixels or in a calibrated unit of measurement (check the correct scale relative to microscope settings under **Image > Properties**). To include everything, keep the default of 0-Infinity and circularity default range at 0.00 – 1.00 (0 = straight line, 1 = perfect circle).

2.2.7.2. To filter small “noise” pixels or features of not interest, set the minimum and maximum range. Tick **Include Holes, Show, Outline** and **Display Results** options in the window field. **Exclude on Edges** will discard particles detected on the borders of the image. **Add to Manager** adds the obtained selection to the ROI manager for further analysis keeping the position information of the particle.

NOTE: In the “ROI Manager”, it is possible to correct automatic segmentation recorded output (merge split cells, split merged cells). Select, by using selection tools in the Fiji Toolbar, ROIs inside both gel regions where cancer cells are embedded to estimate immune infiltration.

2.2.8. Export the obtained values to a spreadsheet to perform statistical analysis as shown in **Figure 7G**. “Results” lists a data table relative to numbered outlined particle properties identified. “Summarize” opens a window with the name of the image, total counts, and other information for the whole image.

2.2.8.1. Go to **Analyze > Set Measurements** to include a wide range of parameters.

2.2.9. Record optionally a macro (by selecting **Plugins > Macros > Record**) to automate the processing workflow and save time analysis on large datasets.

2.2.9.1. Use the same processing routine to analyze green fluorescence channel in the same regions for analyzing morphological changes of tumor cells in 3D regions[16].

REPRESENTATIVE RESULTS:

Tumor immune infiltration is a parameter of the host anti-tumor response. Tumors are heterogeneous in the composition, density, location, and functional state of infiltrating leukocytes which interactions with cancer cells can underlie clinically relevant information to predict disease course and response to therapy. In this sense, microfluidic technologies could be used as complementary and privileged in vitro tools to explore the immune contexture of tumors, as well as to monitor the response to anticancer therapies. The coupling of the microfluidic assay, live-cell imaging, and tracking software may establish reliable quantification methods to quantify how immune cells adjust their migration pattern in different contexts. In this chapter, we have reported steps for setting up versatile 2D or 3D co-cultures of immune and target cancer cells in ad hoc microfluidic devices realized by standard soft-lithographic procedures. In Section 1 microfluidic devices were employed to allow chemical and physical contacts between adherent (MDA-MB-231 cancer cells) and non-adherent (PBMCs) populations. Some chemotherapeutic agents (e.g., anthracyclines among the others) can induce "immunogenic" apoptosis of malignant cells, thus enhance their visibility in immunocompetent hosts. Cancer immunogenic cell death (ICD) is characterized by the release of membrane-bound and soluble signals delivered by dying cells functioning as alarmins for immune cells. To provide a quantitative validation of ICD response, we employ data collected in the microfluidic platform where leukocytes can move through suitably built microchannel bridges toward their target cells. Time-lapse recordings were performed after co-loading PBMCs, from healthy donors (WT, wild type), with human MDA-MB-231 breast cancer cells pre-treated or not with the anthracycline DOXO. Microphotographs were generated every 2 min, for two successive time intervals of 24 and 48 h. (Exemplary **Movie S1** of 0-24 h interval). Tracking analysis of individual PBMCs challenged with dying (DOXO-treated) or live (PBS-treated) cancer cells was done using Trackmate plug-in, as seen in **Figure 6A** (left panel). Relevant chemotaxis values and migration plots were automatically generated by using the Chemotaxis and Migration Tool, as detailed in[62]. The cell trajectories were all extrapolated to (x, y) = 0 at time 24 h. The results indicated a different migratory profile of the immune cells when co-loaded with breast cancer cells exposed to DOXO or PBS. When

PBMCs were confronted with apoptotic cancer cells, they crossed microchannels towards dying/dead cells (but not to live untreated cells). Migration X/Y spider and rose plots, presented in left panel **Figure 6B-C**, were mapped and compared to highlight the impact of immunogenic inducers agents on differences in immune dynamics. Rose plots demonstrate that PBMCs migrated mainly in nearly all directions in the control experiment, only a negligible fraction is guided up the gradient generated by proliferating cancer cells. Conversely, the paths of individual cells highlight a strong bias movement along the direction of apoptotic breast cancer cells (negative x-direction). To evaluate directed immune cell migration towards DOXO-treated or PBS-treated cancer cells, tseveral chemotaxis parameters are computed, including: a) the center of mass (spatial averaged point of all endpoints); b) the directionality; c) the forward migration index (i.e., the average cell displacement in a direction of interest which means towards target tumor site, in our case). The latter values represent a measurement of the cell efficiency of a cell to migrate in the direction given chemotactic stimuli. After reaching the left chamber, a fraction of leukocytes with an increasing density over 24-48 h exhibited a long-term (>60 min) contacts with DOXO-treated MDA-MB-231. PBMCs fail to massively migrate and engage in such long-term and persistent interactions with live cancer cells (as shown by representative microphotographs of approaching PBMCs in **Figure 6A**, right). For quantifying differences in tumor-immune interplay, the tumor region was delineated with a fixed circle of diameter ranging 20-80 microns, named “hotspot”. The quantification and analysis from representative FOVs are shown in **Figure 6** (Right panel, B-C).

In Section 2 a novel 3D immuno-competent tumor model was described to quantify the recruitment of immune cells in response to anti-cancer combinations of epigenetic drugs[32] (DAC/IFN *vs* IFN alone), allowing the comparison of two different treatment conditions of A375 melanoma cells simultaneously. Thus, A375M melanoma cells, labeled with PKH67 green fluorescent dye were embedded in Matrigel matrices in the presence of DAC and/or IFN into each gel chamber, whereas PKH26 red-labeled PBMCs were distributed homogenously into the central fluidic chamber at the starting point (**Figure 7A**). We compared simultaneously the two tumor masses in 3D matrices for their capacity to attract PBMCs. At 48 and 72 h, PBMCs are guided massively into the right-side microchannels, as observed in **Figure 7B**.

A preferential homing of PBMCs toward the gel matrix containing DAC/IFN-treated, rather than IFN-treated, melanoma site was clearly observed, whereas poor migration rate was visible toward A375 cells exposed to single treatment (left chip side). The competitive setting is applicable to investigate a plethora of different cancer biology phenotypes (e.g., drug-resistant *vs* aggressive, primary or metastatic (e.g., A375P *vs* A375M melanoma cells), and responders *vs* non-responders). Gel chambers can be comprised of complex co-cultures of malignant cells and multiple non-cancerous tumor-associated cells, such as endothelial cells, immune cells, and fibroblasts[33] to characterize TME-level drug responses. Events of mitosis and apoptotic death of cancer cells can be monitored by staining with live dyes[33]. Immunostaining procedures on 3D microfluidic devices could be adapted to evaluate states of activation of infiltrated immune cells in tumor sites by confocal microscopy[35]. In this sense, these 3D microfluidic systems may mimic complex tumor structures and multicellular interactions and therefore are valuable platforms for more reliable preclinical drug testing.

FIGURE AND TABLE LEGENDS:

Figure 1. Planimetry of the microfluidic device for assembling 2D tumor-immune co-cultures. (A) Real microphotograph of 3 chips assembled into a single microscope slide. The reservoirs are numbered depending on the loading sequence and are color-coded as the corresponding culture chambers listed in the legend. Scalebar, 6 mm. (B) Details of the narrow microgrooves bridge, showing the dimensions tailored to cancer cells and PBMCs size. C) 3D CAD of chip consisting of three main cell culture areas connected by microgrooves. D-E) Visible light microphotograph was acquired before the beginning of the time-lapse, showing the distribution of cancer cells and PBMCs respectively in the left and the intermediate chamber. Scalebar, 500 µm.

Figure 2. Trackmate analysis pipeline for localization of immune spots in time-series images. A) Upper panel: Screenshot of Trackmate image calibration menu. Lower panel: Fiji "Image properties menu" to set time and spatial units. B) Upper panel: Screenshot of Trackmate image calibration menu. Lower panel: Output image with applied different values of "Threshold". -C) Upper panel: Screenshot of Trackmate "Spot filtering" menu illustrating some filters. Lower panel: Exemplary time-lapse image, depicting immune spots filtered by position along X in the intermediate chamber.

Figure 3. Trackmate Analysis pipeline for reconstructing immune tracks in time-series image sequences. A-C) Screenshots of Trackmate menus corresponding to detector selection for track building, track filtering, and to display menus for exporting final data. D) Examples of generated tracks in pre-processed time-lapse images varying the linking detector settings. E) Example of false tracks and bad links derived from the detection of tumor cells borders. F) Tracks are highlighted in green by selecting rows in the file .txt of results.

Figure 4. Schematic overview for 3D immunocompetent tumor-on chips. A) Examples of micro-structured silicon master. Stamps for PDMS were patterned in SU-8 negative resist in a cleanroom facility equipped with e-beam and optical lithography. B) Polydimethylsiloxane (PDMS) replicas were fabricated by standard soft-lithography methods. The central unit has the chambers colored as the ones drawn in 3D rendering of the chip, depicted in the panel D. C) Scanning electron microscopy (SEM) enlarged view of the array of micropillars suited for hydrogel solution entrapment. D)3D CAD showing the chambers, connected by microgrooves and the loading wells. Dashed boxes are referred to SEM photographs of details (panel C, and E). E) SEM photograph of 10 µm high connecting microgrooves. F) 2D CAD layout depicting the dimensions of microstructures.

Figure 5. Schematic workflow of main loading protocol steps for assembling 3D co-cultures. A) Upper panel: Schematics of injection step of Matrigel solution in each gel side region. Lower panel: Real photograph of the chip showing gel front advancement along the channel during loading step. B) Schematics of Matrigel polymerization step. Lower panel: Phase-contrast microscopic view of the gel-air interface formed after gelation step. Scalebar, 100 µm. C)Upper panel: Drawing, depicting the loading of cells and media with exemplary volumes used in the protocol. Lower panel: 4X Phase-contrast image of the assembled co-culture at 0h is shown in lower panel. Scalebar, 200 µm.

Figure 6. Analysis of migratory profiles and interaction behavior of PBMC towards

dying/live tumor chamber in the time window of 24-48 h. Left panel. A) Screenshots of time-lapse pre-processed images overlaid with immune colored tracks, extracted by Trackmate. The immune paths are obtained by a single FOV in the indicated experimental conditions in the interval 24-to-48 h in the intermediate chamber. B-C) Representative migration tracks and rose plots of PBMCs cultivated in the two different conditions (*n* = 1550 PBMCs versus DOXO-treated cancer cells, DOXO+ or *n* =1434 PBMCs versus control cancer cells, DOXO-). Each line inside x-y plots depicts a single PBMC trajectory and each circle represents the final position of a single cell with respect to the initial position. Starting points are set to (0,0) using a coordinate transformation. The coordinates and displacement of the center of mass of cell migration are displayed in the indicated experimental conditions. The center of mass coordinates and displacement (computed as average Euclidean distance for the X and Y components) provide indication of the average direction in which the group of cells primarily travelled and magnitude of the overall cell movement in condition groups. Blue and green lines respectively mark individual tracks by Euclidean distance value greater/smaller than a threshold value (100 µm). D) Scheme of numerical data extracted by a cell track. E-F) Box & Whiskers plot depicting respectively directionality ($p<0,0001$ Unpaired *t* test with Welch's correction) and FMI ($p<0,0001$ Unpaired *t* test with Welch's correction). The horizontal line in boxes represents median values. The FMI values are the average for all cell-tracks in each condition group.

Right panel. A) Screenshots of Trackmate extracted ROIs showing differential interactions between PBMCs and DOXO or PBS-treated cancer cells. B) Time density of PBMCs around DOXO-treated or control MDA-MB-231 cancer cells. Number of PBMCs present into selected ROI around cancer cells for each condition. Values reported are the average over 9 selected ROI from a single time-lapse FOV. Cancer hotspots are defined in a ROI (80 µm on in diameter). Corresponding density heatmap is displayed. Dots represent mean number of cells calculated over 9 cancer hotspots at indicated time points. C) Distribution of times (min) of contacts for each experimental group.

Figure 7. Preferential recruitment of PBMCs in response to DAC plus IFN drug combinations in a competitive 3D immuno-competent melanoma on chip model. A) Distribution of initially loaded PBMCs in the central chamber of microfluidic devices. Microphotographs are acquired by EVOS-FL fluorescence microscope during 0-72 h interval. Red fluorescence (PKH67-labeled cells) represents PBMCs from healthy donors. PKH67-labeled (green) human melanoma cells embedded in Matrigel containing single or double combinations treatments were plated in lateral chambers. B) A375 cells plus IFN on left versus A375 plus DAC/IFN on the right. Fluorescence images were shown at 72 h of co-culture. Discontinued yellow box depicts visibly massive recruitment in A375 plus DAC/IFN side. C) PBMC counts in four different ROIs from IFN chambers *vs* DAC+IFN chambers. Histograms represent cell counts +/- S.D.; heatmap enumerated values from each ROI. Scalebars, 200 µm. D-G) Schematics of segmentation and quantification steps of infiltrated PBMCs in gel matrices applied to single channel fluorescence images.

Supplementary File. Microfabrication protocol

Supplementary Movie 1. Time-lapses sequences in a 2D tumor-immune on-chip co-culture. Microphotographs were acquired every 2 min, in a time interval of 0-24 h by means of a smart Microscope into a standard cell culture incubator. Left panel. Movie of PBMCs from healthy

donors (WT, wild type), plated with MDA-MB-231 control breast cancer cells. Right panel. Movie of a massive migration of PBMCs WT towards the chip chamber where MDA-MB-231 DOXO-treated cancer cells, are loaded. 2D chip layout is described in detail in section 1of Protocol and shown in Figure 1.

DISCUSSION

The described methods try to design a general approach to recapitulate, with modulable degree of complexity, two significant aspects in the field of onco-immunology, which can benefit from the adoption of more relevant in vitro models. The first one involves the tumor cell population side, where tackling single cell characteristics may lead to a better description of heterogeneity and correlated biological and clinical significance including resistance to therapy, propension to metastasis, stem cell and differentiation grade. The other side of the story is represented by the TME, including noncancerous components (immune and stromal cells, blood vessels) and chemical/physical landscape (ECM constituents, chemokines and other soluble factors released) that can profoundly shape both the characteristics of the disease and individual's response to therapy[63], particularly to immunotherapy. It is worth to note that exporting the described approach to other research fields requires a deep understanding of limitations and challenges brought by the development and adoption of new models.

Quoting a maxim applied in engineering modelling ("model the problem not the system"), it must be optimized which is the minimum number of (cellular, physical and chemical) components and conditions needed to make own on-chip model biologically relevant and stable along the whole experiment. Every combination of cell types/microenvironmental/experimental setting must, thus, be accurately chosen, evaluated, and continuously monitored along single experiments and from session to session. These checks include, as mentioned in the protocol sections, strict control of parameters like volumes in the microfluidic devices that can be modified by humidity conditions or heating from illumination sources, possible movements and non-planarity of stages causing uncontrolled liquid drifts, but also some endpoint verification of cell state, viability and phenotypic characterization. One critical step concerns the decision to use perfusion systems to create vascularized (like) structures, or for on-chip drug delivery[33], since this may affect the experiments in terms of increasing complexity, cell culture duration, and modulation of the chemical factors in presence of floating cells like the immune ones.

In the following, we summarize the main critical and relevant issues found in the experimental settings and in the most recent literature.

ECM and chemical landscape definition

TME is deeply affected also by the mechanical[64,65] properties of the surroundings[63, 66]. For this reason, the choice of the culturing matrix is fundamental, especially when dealing with immune cells that, in certain conditions, could respond to signals released by the matrix itself. Relevant advances are expected in the next future also from design and development of new materials and hydrogels (featured by different stiffness, porosity, presence of soluble factors, among the other parameters) that are enabling an increasingly refined and controllable ECM, mimicking specificities of different tissues today, different patients tomorrow. On the other side is also critical to monitor the changes induced by the different cell populations in the

ECM and define strategies to include this information in dynamic and phenotypic analyses.

Data management

The path toward deployment of tumor on-chip techniques in a clinical workflow is going to benefit from a huge experimental work that is taking place along several directions. Organ-on-chip models, as many in vitro techniques, are functional, at least potentially, to perform high-throughput/high-content measurements. Parallelization of experimental conditions, including positive and negative controls, and technical/biological replicates is made possible by integrating several chips on the same plate. The increase in the quantitative throughput plays a crucial role in translating and validating these systems in fast drug or gene screening pipeline for immunotherapies. Indeed, several companies have already developed platforms in a multi-well format, and different imaging approaches are being tested to allow for monitoring a high number of devices simultaneously[14]. In the above described protocols, we used microscope slides allocating up to 3 chips, with the possibility to visualize up to 12 experimental conditions in parallel, using a standard microscope multi-slide tray. This setup is compatible with hand pipetting and suitable for custom oriented adjustments performed in our microfabrication facility. On the contrary, when a strong parallelization is necessary (multiple screening tests and controls), setup optimizations to set a higher level of automation (i.e., use of pipetting robots, plastic multi-wells) are required.

When designing experiments, a trade-off between spatial and temporal resolution must be taken in account.

The huge amount of data, produced by high content microscopy, constitutes a limiting factor in terms of storage, transfer and analysis. These issues are being addressed with computational approaches implementing machine learning tools and hardware/software resources, which may foster the future possibility to link on-chip/in-silico experiments[67,68] in choosing therapeutic strategies, and that represents an ambitious yet non-deferrable opportunity.

Beyond Fluorescence Imaging

Fluorescence labelling, by dyes or reporter genes, due to its high specificity, undoubtedly represents the gold standard method to identify different cell populations in co-culture conditions and to resolve molecular properties with high SNR. In OOC models this approach is commonly used as a reference and particularly in heterogeneous tumor-on-chip microenvironments, it can be valuable to characterize the phenotype of immune cells infiltrated and interacting.

Nevertheless, there is increasing evidence that effects induced by fluorophores, laborious staining procedures and illumination routines must be monitored and minimized[69] because can deeply affect cell behavior and state[70,71]. This risk seems particularly true for fragile systems, such as immune cells[72,73]. Phototoxic reactions may introduce limitations in defining the temporal window acquisition of live cells when monitored at high spatial and temporal resolution. Moreover, the richness in the variety of immune sub-populations make unfeasible to discriminate among them only by fluorescent staining, considering the limited number of filters commonly available on microscopes.

To address this issue, from an instrumental point of view, novel label free[74] microscopy techniques such as holographic[56] or hyperspectral microscopy[57] are now appearing on the stage. They promise advanced cellular process classification strategies beyond fluorescence and can be particularly valuable for studying sensitive samples. From a data analysis point of view, advanced computational approaches, based on deep learning algorithms[75] (trained by fluorescence images datasets), are door-openers to perform the so called "in silico labeling"[76,77]. They have been successfully applied to predict fluorescent markers from bright-field images[78], generating labeled images, without staining cells, thus increasing bright field microscopy informative power. This strategy can also be useful to save time and fluorescence channels for other markers. We believe that OOC community will benefit from these new techniques allowing a less invasive study of cell populations interaction.

Data analysis

Mechanisms of interactions between immune and target cancer cells can be investigated through tracking of cell movements[28,79]. Time-lapse tracking experiments in complex and heterogeneous co-cultures are extremely valuable to extract cell migration patterns, morphological and state changes, and comprehensive lineage information. Performing manual analysis is practically only feasible for short sequences with few cells but not for high-throughput, systematic experiments. Consequently, the development of computational tools for cell tracking, either fully or partly automated, is a vital field of research in image analysis[24]. Typically, conventional cell tracking requires relatively high frequency of sampling and spatial resolution to correctly perform segmentation tasks, which can be challenging in many experimental conditions. To localize cells, there are available open-access segmentation and tracking tools (e.g., ImageJ software[22]) as presented in this protocol or dedicated proprietary software. In large-scale studies, we applied a proprietary software called *Cell Hunter*[16,31], developed by University of Tor Vergata in Rome, to distinguish in a fully automatic way cancer and immune cells in multi-population context. Tailor-made solutions based on machine learning and Neural network approaches[80–82] are beginning to be today implemented in microscopy software packages[83], from improving SNR to managing critical acquisition parameters or segmentation steps. Machine learning can be exploited to recognize common cellular patterns (e.g., motion styles) in order to characterize the biological response with respect to microenvironmental factors.

In Comes et al.[41], a pre-trained Deep Learning Convolutional Neural Network architecture was applied to classify if cancer cells are or not exposed to a drug treatment by using as a "marker" the motility of the immune cells, tracked from time-lapse data of co-cultures of breast cancer cells and PBMCs in collagen matrices in microdevices, as described in[33].

Single-cell omics methods and ontologies development

We point out the need for a strategic alliance between single-cell omics technologies[84] (e.g., proteomics, metabolomics, genomics) and on-chip methods: the molecular detailed characterization, conjugated to functional dynamic information could enhance comprehension of basic mechanisms and clinical description. In this case new instruments for linking the two worlds are at their beginning[85]. The first challenge is to implement single-cell omics approaches directly on the onco-immunology chips[22]. Moreover, organ-on-chips could be exploited as platforms to test potential targets identified by genomics and proteomics analyses[86,87]. A second linking tool, which is still largely missing, is a structured, standardized

way of annotating and storing measured system results[88,89]. But this is exactly what we need in the future to build systematic databases of cellular quantitative results and measured characteristics, to mine, infer and correlate them with the inherent biological information. In a word, the need for standardization and systematic analysis of heterogeneous experimental datasets calls for an ontology framework.

Personalizing models

Organs-on-chip technology is suitable for personalization[12], since cells and tissues from single patients (or classes of patients) can be used in the devices under controlled conditions, leading to clinically relevant readouts, useful to inform therapeutic or prevention strategies. Some examples are starting to appear in literature[90]. Of course, for tumor-on-chip models, this challenge poses several technical and scientific questions to be solved[36] (like TME characteristics control such as oxygen concentration, cytokine gradients, etc). Importantly, the prospect of making oncology and onco-immunology therapies more effective while reducing harmful effects for each patient is attractive, from a quality of life perspective as for the optimization of healthcare resources.

In conclusion, it is apparent that this field is an authentically interdisciplinary one and as such, requires a great effort in establishing a common language and shared goals between researcher, clinicians, industry, but also from different disciplines (engineering, biology, data science, medicine, chemistry) finding good balance and new solutions[91].

DISCLOSURES:

The authors have nothing to disclose. AS is supported by the Fondazione Italiana per la Ricerca sul Cancro (AIRC, Start-Up 2016 #18418) and Ministero Italiano della Salute (RF_GR-2013-02357273). GS and FM are supported by the Italian Association for Cancer Research (AIRC) no. 21366 to G.S.).

REFERENCES:

1. Abul K. Abbas, A.H.L. and S.P. *Cellular and Molecular Immunology, Ninth Edition*. *Cellular and Molecular Immunology*. (2018).
2. Eisenstein, M. Cellular censuses to guide cancer care. *Nature*. doi: 10.1038/d41586-019-00904-5 (2019).
3. Models for Immuno-oncology Research. *Cancer Cell*. doi: 10.1016/j.ccell.2020.07.010 (2020).
4. Zhang, Z. et al. Morphology-based prediction of cancer cell migration using an artificial neural network and a random decision forest. *Integrative biology : quantitative biosciences from nano to macro*. **10** (12), 758–767 (2018).
5. Dagogo-Jack, I., Shaw, A.T. Tumour heterogeneity and resistance to cancer therapies. *Nature Reviews Clinical Oncology*. **15** (2), 81–94 (2018).
6. Milo, I. et al. The immune system profoundly restricts intratumor genetic heterogeneity. *Science Immunology*. **3** (29), eaat1435 (2018).
7. Mlecnik, B. et al. The tumor microenvironment and Immunoscore are critical determinants of dissemination to distant metastasis. *Science Translational Medicine*. doi: 10.1126/scitranslmed.aad6352 (2016).
8. Sbarrato, T. et al. 34th Annual Meeting & Pre-Conference Programs of the Society for Immunotherapy of Cancer (SITC 2019): part 1. *Journal for ImmunoTherapy of Cancer*. **7**

(Suppl 1), 282 (2019).
9. Miller, C.P., Shin, W., Ahn, E.H., Kim, H.J., Kim, D.-H. Engineering Microphysiological Immune System Responses on Chips. *Trends in Biotechnology*. **38** (8), 857–872 (2020).
10. Ma, C., Harris, J., Morales, R.-T.T., Chen, W. Microfluidics for Immuno-oncology. *Nanotechnology and Microfluidics*. 149–176 (2020).
11. Mengus, C. et al. In vitro Modeling of Tumor–Immune System Interaction. *ACS Biomaterials Science & Engineering*. **4** (2), 314–323 (2018).
12. Van Den Berg, A., Mummery, C.L., Passier, R., Van der Meer, A.D. Personalised organs-on-chips: functional testing for precision medicine. *Lab on a Chip*. doi: 10.1039/c8lc00827b (2019).
13. Ingber, D.E. Reverse Engineering Human Pathophysiology with Organs-on-Chips. *Cell*. doi: 10.1016/j.cell.2016.02.049 (2016).
14. Huh, D. et al. Microfabrication of human organs-on-chips. *Nature Protocols*. doi: 10.1038/nprot.2013.137 (2013).
15. Mazzarda, F. et al. Organ-on-chip model shows that ATP release through connexin hemichannels drives spontaneous Ca2+ signaling in non-sensory cells of the greater epithelial ridge in the developing cochlea. *Lab Chip*. doi: 10.1039/D0LC00427H (2020).
16. Mencattini, A. et al. High-throughput analysis of cell-cell crosstalk in ad hoc designed microfluidic chips for oncoimmunology applications. *Methods in Enzymology*. **632**, 479–502 (2020).
17. Maharjan, S., Cecen, B., Zhang, Y.S. 3D Immunocompetent Organ-on-a-Chip Models. *Small Methods*. **n/a** (n/a), 2000235 (2020).
18. Phan, D.T.T. et al. A vascularized and perfused organ-on-a-chip platform for large-scale drug screening applications. *Lab on a Chip*. doi: 10.1039/c6lc01422d (2017).
19. Jeon, J.S., Zervantonakis, I.K., Chung, S., Kamm, R.D., Charest, J.L. In vitro Model of Tumor Cell Extravasation. *PLoS ONE*. doi: 10.1371/journal.pone.0056910 (2013).
20. Jeon, J.S. et al. Human 3D vascularized organotypic microfluidic assays to study breast cancer cell extravasation. *Proceedings of the National Academy of Sciences of the United States of America*. doi: 10.1073/pnas.1417115112 (2015).
21. Chen, M.B., Whisler, J.A., Fröse, J., Yu, C., Shin, Y., Kamm, R.D. On-chip human microvasculature assay for visualization and quantification of tumor cell extravasation dynamics. *Nature Protocols*. doi: 10.1038/nprot.2017.018 (2017).
22. Sade-Feldman, M. et al. Defining T Cell States Associated with Response to Checkpoint Immunotherapy in Melanoma. *Cell*. doi: 10.1016/j.cell.2018.10.038 (2018).
23. Di Modugno, F., Colosi, C., Trono, P., Antonacci, G., Ruocco, G., Nisticò, P. 3D models in the new era of immune oncology: Focus on T cells, CAF and ECM. *Journal of Experimental and Clinical Cancer Research*. doi: 10.1186/s13046-019-1086-2 (2019).
24. Svensson, C.-M., Medyukhina, A., Belyaev, I., Al-Zaben, N., Figge, M.T. Untangling cell tracks: Quantifying cell migration by time lapse image data analysis. *Cytometry. Part A : the journal of the International Society for Analytical Cytology*. **93** (3), 357–370 (2018).
25. Arena, E.T., Rueden, C.T., Hiner, M.C., Wang, S., Yuan, M., Eliceiri, K.W. Quantitating the cell: turning images into numbers with ImageJ. *Wiley interdisciplinary reviews. Developmental biology*. **6** (2) (2017).
26. Schindelin, J. et al. Fiji: An open-source platform for biological-image analysis. *Nature Methods*. doi: 10.1038/nmeth.2019 (2012).
27. Vacchelli, E. et al. Chemotherapy-induced antitumor immunity requires formyl peptide receptor 1. *Science*. **350** (6263), 972 LP – 978 (2015).

28. Businaro, L. et al. Cross talk between cancer and immune cells: exploring complex dynamics in a microfluidic environment. *Lab on a Chip*. **13** (2), 229–239 (2013).
29. Beltman, J.B., Marée, A.F.M., de Boer, R.J. Analysing immune cell migration. *Nature Reviews Immunology*. **9** (11), 789–798 (2009).
30. Agliari, E. et al. Cancer-driven dynamics of immune cells in a microfluidic environment. *Scientific Reports*. **4** (1), 6639 (2014).
31. Biselli, E. et al. Organs on chip approach: a tool to evaluate cancer -immune cells interactions. *Scientific Reports*. **7** (1), 12737 (2017).
32. Lucarini, V. et al. Combining Type I Interferons and 5-Aza-2′-Deoxycitidine to Improve Anti-Tumor Response against Melanoma. *Journal of Investigative Dermatology*. **137** (1), 159–169, doi: 10.1016/J.JID.2016.08.024 (2017).
33. Nguyen, M. et al. Dissecting Effects of Anti-cancer Drugs and Cancer-Associated Fibroblasts by On-Chip Reconstitution of Immunocompetent Tumor Microenvironments. *Cell Reports*. **25** (13), 3884-3893.e3, doi: 10.1016/J.CELREP.2018.12.015 (2018).
34. Racioppi, L. et al. CaMKK2 in myeloid cells is a key regulator of the immune-suppressive microenvironment in breast cancer. *Nature Communications*. **10** (1), 2450, doi: 10.1038/s41467-019-10424-5 (2019).
35. Parlato, S. et al. 3D Microfluidic model for evaluating immunotherapy efficacy by tracking dendritic cell behaviour toward tumor cells. *Scientific Reports*. **7** (1), 1093, doi: 10.1038/s41598-017-01013-x (2017).
36. Andreone, S. et al. IL-33 Promotes CD11b/CD18-Mediated Adhesion of Eosinophils to Cancer Cells and Synapse-Polarized Degranulation Leading to Tumor Cell Killing. *Cancers*. **11** (11), 1664, doi: 10.3390/cancers11111664 (2019).
37. Bray, L.J., Hutmacher, D.W., Bock, N. Addressing Patient Specificity in the Engineering of Tumor Models. *Frontiers in Bioengineering and Biotechnology*. **7**, 217, doi: 10.3389/fbioe.2019.00217 (2019).
38. Fetah, K.L. et al. Cancer Modeling-on-a-Chip with Future Artificial Intelligence Integration. *Small*. **15** (50), 1901985 (2019).
39. Jabbari, P., Rezaei, N. Artificial intelligence and immunotherapy. *Expert Review of Clinical Immunology*. **15** (7), 689–691 (2019).
40. Mak, K.-K., Pichika, M.R. Artificial intelligence in drug development: present status and future prospects. *Drug Discovery Today*. **24** (3), 773–780 (2019).
41. Mencattini, A. et al. Discovering the hidden messages within cell trajectories using a deep learning approach for in vitro evaluation of cancer drug treatments. *Scientific Reports*. doi: 10.1038/s41598-020-64246-3 (2020).
42. Isozaki, A. et al. AI on a chip. *Lab Chip*. doi: 10.1039/D0LC00521E (2020).
43. Makaryan, S.Z., Cess, C.G., Finley, S.D. Modeling immune cell behavior across scales in cancer. *Wiley Interdisciplinary Reviews: Systems Biology and Medicine*. doi: 10.1002/wsbm.1484 (2020).
44. Mak, K.K., Pichika, M.R. Artificial intelligence in drug development: present status and future prospects. *Drug Discovery Today*. doi: 10.1016/j.drudis.2018.11.014 (2019).
45. Masuzzo, P., Van Troys, M., Ampe, C., Martens, L. Taking Aim at Moving Targets in Computational Cell Migration. *Trends in Cell Biology*. **26** (2), 88–110 (2016).
46. Meijering, E., Dzyubachyk, O., Smal, I. Chapter nine - Methods for Cell and Particle Tracking. *Imaging and Spectroscopic Analysis of Living Cells*. **504**, 183–200 (2012).
47. Riedhammer, C., Halbritter, D., Weissert, R. Peripheral blood mononuclear cells: Isolation, freezing, thawing, and culture. *Methods in Molecular Biology*. doi:

10.1007/7651_2014_99 (2015).
48. Harris, J. et al. Fabrication of a microfluidic device for the compartmentalization of neuron soma and axons. *Journal of Visualized Experiments*. doi: 10.3791/261 (2007).
49. Shin, Y. et al. Microfluidic assay for simultaneous culture of multiple cell types on surfaces or within hydrogels. *Nature Protocols*. doi: 10.1038/nprot.2012.051 (2012).
50. Park, J.W., Vahidi, B., Taylor, A.M., Rhee, S.W., Jeon, N.L. Microfluidic culture platform for neuroscience research. *Nature Protocols*. doi: 10.1038/nprot.2006.316 (2006).
51. Gjorevski, N. et al. Neutrophilic infiltration in organ-on-a-chip model of tissue inflammation. *Lab on a Chip*. doi: 10.1039/d0lc00417k (2020).
52. Jenkins, R.W. et al. Ex vivo profiling of PD-1 blockade using organotypic tumor spheroids. *Cancer Discovery*. doi: 10.1158/2159-8290.CD-17-0833 (2018).
53. Comes, M.C. et al. The influence of spatial and temporal resolutions on the analysis of cell-cell interaction: a systematic study for time-lapse microscopy applications. *Scientific Reports*. **9** (1), 6789 (2019).
54. Tinevez, J.-Y. et al. TrackMate: An open and extensible platform for single-particle tracking. *Methods*. **115**, 80–90 (2017).
55. Ulman, V. et al. An objective comparison of cell-tracking algorithms. *Nature Methods*. doi: 10.1038/nmeth.4473 (2017).
56. Tinevez, J.-Y., Herbert, S. The NEMO Dots Assembly: Single-Particle Tracking and Analysis BT - Bioimage Data Analysis Workflows. 67–96 (2020).
57. Jacquemet, G., Hamidi, H., Ivaska, J. Filopodia quantification using filoquant. *Methods in Molecular Biology*. doi: 10.1007/978-1-4939-9686-5_16 (2019).
58. Caldas, P., Radler, P., Sommer, C., Loose, M. Computational analysis of filament polymerization dynamics in cytoskeletal networks. *Methods in Cell Biology*. doi: 10.1016/bs.mcb.2020.01.006 (2020).
59. Chalfoun, J., Majurski, M., Peskin, A., Breen, C., Bajcsy, P., Brady, M. Empirical gradient threshold technique for automated segmentation across image modalities and cell lines. *Journal of Microscopy*. **260** (1), 86–99 (2015).
60. Huang, C.P. et al. Engineering microscale cellular niches for three-dimensional multicellular co-cultures. *Lab on a Chip*. doi: 10.1039/b818401a (2009).
61. Farahat, W.A. et al. Ensemble analysis of angiogenic growth in three-dimensional microfluidic cell cultures. *PLoS ONE*. doi: 10.1371/journal.pone.0037333 (2012).
62. Zengel, P., Nguyen-Hoang, A., Schildhammer, C., Zantl, R., Kahl, V., Horn, E. μ-Slide Chemotaxis: A new chamber for long-term chemotaxis studies. *BMC Cell Biology*. doi: 10.1186/1471-2121-12-21 (2011).
63. Henke, E., Nandigama, R., Ergün, S. Extracellular Matrix in the Tumor Microenvironment and Its Impact on Cancer Therapy. *Frontiers in Molecular Biosciences*. doi: 10.3389/fmolb.2019.00160 (2020).
64. Wirtz, D., Konstantopoulos, K., Searson, P.C. The physics of cancer: The role of physical interactions and mechanical forces in metastasis. *Nature Reviews Cancer*. doi: 10.1038/nrc3080 (2011).
65. Northcott, J.M., Dean, I.S., Mouw, J.K., Weaver, V.M. Feeling stress: The mechanics of cancer progression and aggression. *Frontiers in Cell and Developmental Biology*. doi: 10.3389/fcell.2018.00017 (2018).
66. Wan, L., Neumann, C.A., LeDuc, P.R. Tumor-on-a-chip for integrating a 3D tumor microenvironment: chemical and mechanical factors. *Lab Chip*. **20** (5), 873–888 (2020).
67. Braun, E., Bretti, G., Natalini, R. Mass-preserving approximation of a chemotaxis multi-

domain transmission model for microfluidic chips. *ArXiv*. **abs/2007.1** (2020).
68. Mahlbacher, G.E., Reihmer, K.C., Frieboes, H.B. Mathematical modeling of tumor-immune cell interactions. *Journal of Theoretical Biology*. doi: 10.1016/j.jtbi.2019.03.002 (2019).
69. Magidson, V., Khodjakov, A. Circumventing photodamage in live-cell microscopy. *Methods in Cell Biology*. doi: 10.1016/B978-0-12-407761-4.00023-3 (2013).
70. Jensen, E.C. Use of Fluorescent Probes: Their Effect on Cell Biology and Limitations. *Anatomical Record*. doi: 10.1002/ar.22602 (2012).
71. Skylaki, S., Hilsenbeck, O., Schroeder, T. Challenges in long-term imaging and quantification of single-cell dynamics. *Nature Biotechnology*. doi: 10.1038/nbt.3713 (2016).
72. Abbitt, K.B., Rainger, G.E., Nash, G.B. Effects of fluorescent dyes on selectin and integrin-mediated stages of adhesion and migration of flowing leukocytes. *Journal of Immunological Methods*. doi: 10.1016/S0022-1759(00)00189-7 (2000).
73. Smith, E. et al. Phototoxicity and fluorotoxicity combine to alter the behavior of neutrophils in fluorescence microscopy based flow adhesion assays. *Microscopy Research and Technique*. doi: 10.1002/jemt.20362 (2006).
74. Suman, R. et al. Label-free imaging to study phenotypic behavioural traits of cells in complex co-cultures. *Scientific Reports*. doi: 10.1038/srep22032 (2016).
75. Brent, R., Boucheron, L. Deep learning to predict microscope images. *Nature Methods*. doi: 10.1038/s41592-018-0194-9 (2018).
76. Christiansen, E.M. et al. In Silico Labeling: Predicting Fluorescent Labels in Unlabeled Images. *Cell*. doi: 10.1016/j.cell.2018.03.040 (2018).
77. Waibel, D.J.E., Tiemann, U., Lupperger, V., Semb, H., Marr, C. In-silico staining from bright-field and fluorescent images using deep learning. *Lecture Notes in Computer Science (including subseries Lecture Notes in Artificial Intelligence and Lecture Notes in Bioinformatics)*. doi: 10.1007/978-3-030-30508-6_15 (2019).
78. Ounkomol, C., Seshamani, S., Maleckar, M.M., Collman, F., Johnson, G.R. Label-free prediction of three-dimensional fluorescence images from transmitted-light microscopy. *Nature Methods*. doi: 10.1038/s41592-018-0111-2 (2018).
79. Diehl, M.I., Wolf, S.P., Bindokas, V.P., Schreiber, H. Automated cell cluster analysis provides insight into multi-cell-type interactions between immune cells and their targets. *Experimental Cell Research*. **393** (2), 112014 (2020).
80. Chen, H., Engkvist, O., Wang, Y., Olivecrona, M., Blaschke, T. The rise of deep learning in drug discovery. *Drug Discovery Today*. doi: 10.1016/j.drudis.2018.01.039 (2018).
81. Angermueller, C., Pärnamaa, T., Parts, L., Stegle, O. Deep learning for computational biology. *Molecular Systems Biology*. doi: 10.15252/msb.20156651 (2016).
82. Moen, E., Bannon, D., Kudo, T., Graf, W., Covert, M., Van Valen, D. Deep learning for cellular image analysis. *Nature Methods*. doi: 10.1038/s41592-019-0403-1 (2019).
83. No Title. https://www.microscope.healthcare.nikon.com/produc.
84. Bock, C., Farlik, M., Sheffield, N.C. Multi-Omics of Single Cells: Strategies and Applications. *Trends in Biotechnology*. doi: 10.1016/j.tibtech.2016.04.004 (2016).
85. Lin, A. et al. 3D cell culture models and organ-on-a-chip: Meet separation science and mass spectrometry. *Electrophoresis*. doi: 10.1002/elps.201900170 (2020).
86. Ingber, D.E. Developmentally inspired human 'organs on chips.' *Development (Cambridge)*. doi: 10.1242/dev.156125 (2018).
87. Low, L.A., Mummery, C., Berridge, B.R., Austin, C.P., Tagle, D.A. Organs-on-chips: into the next decade. *Nature Reviews Drug Discovery*. doi: 10.1038/s41573-020-0079-3 (2020).

88. Mangul, S. et al. Systematic benchmarking of omics computational tools. *Nature Communications*. doi: 10.1038/s41467-019-09406-4 (2019).
89. Burek, P., Scherf, N., Herre, H. Ontology patterns for the representation of quality changes of cells in time. *Journal of Biomedical Semantics*. **10** (1), 16 (2019).
90. Benam, K.H. et al. Small airway-on-a-chip enables analysis of human lung inflammation and drug responses in vitro. *Nature Methods*. doi: 10.1038/nmeth.3697 (2016).
91. Horning, S.J. A new cancer ecosystem. *Science*. doi: 10.1126/science.aan1295 (2017).

Figure

Click here to access/download;Figure;figure01_300dpi.tif

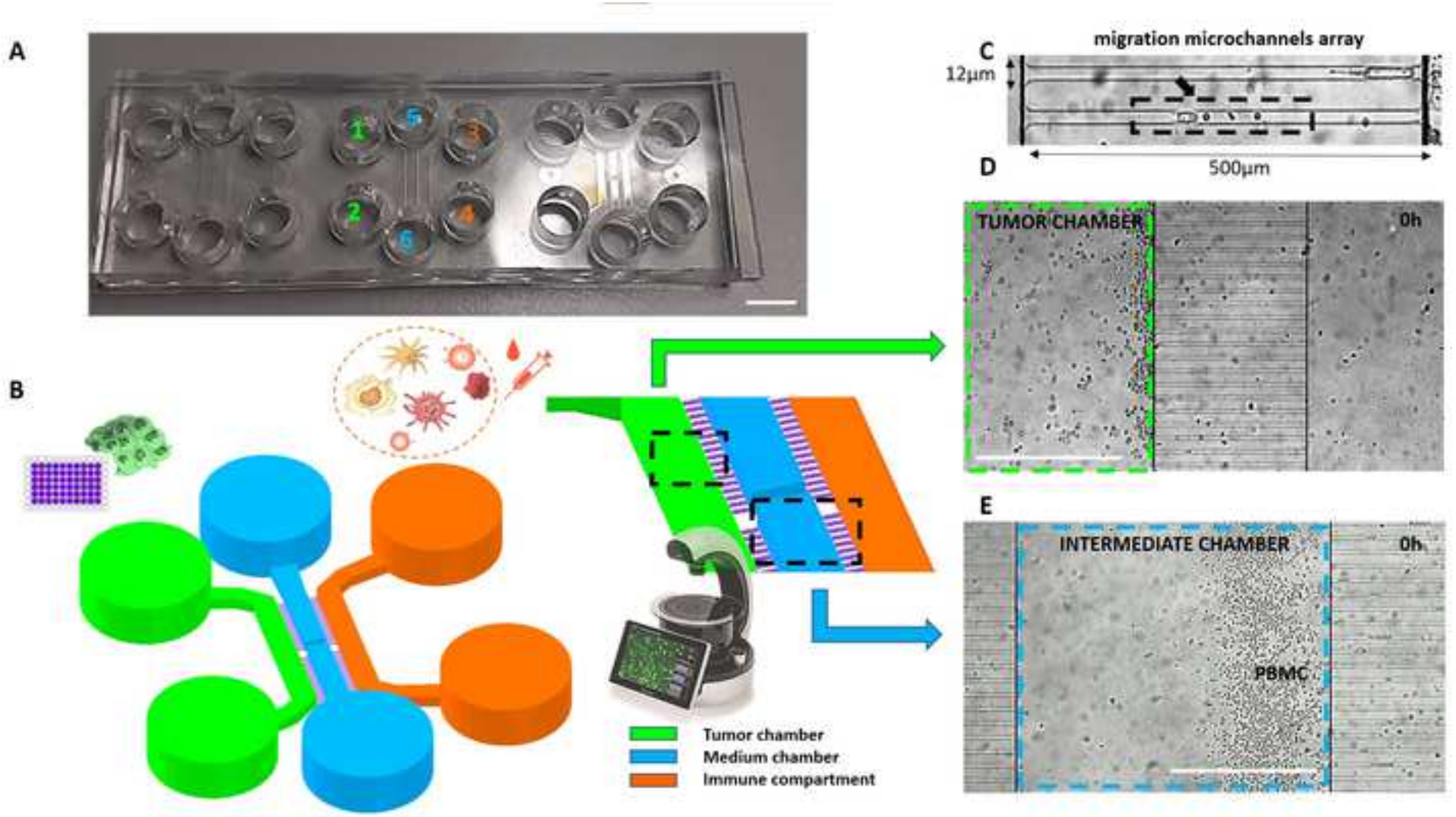

figure01.jpg

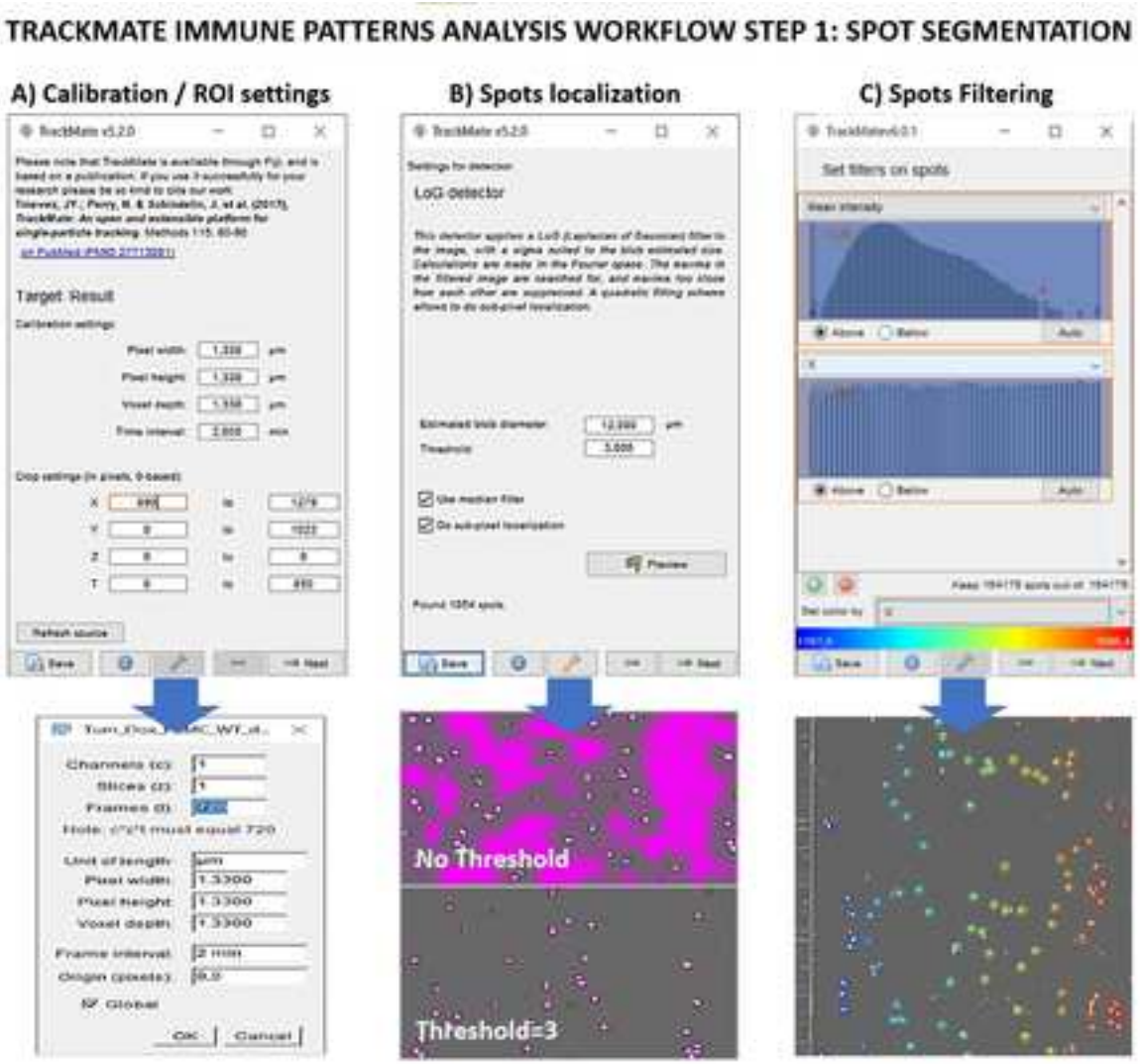

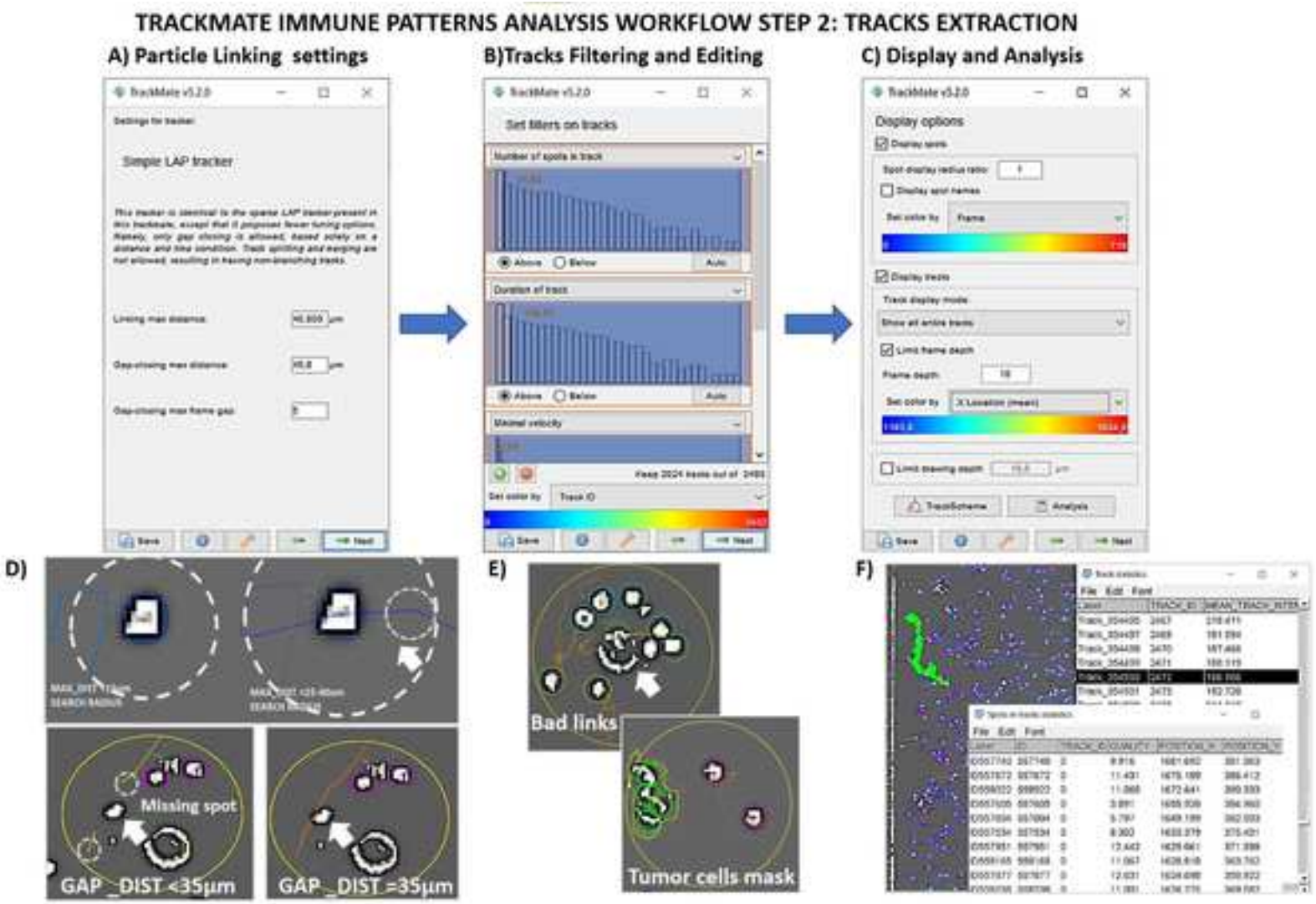

Figure

Click here to access/download;Figure;figure04_300dpi.tif

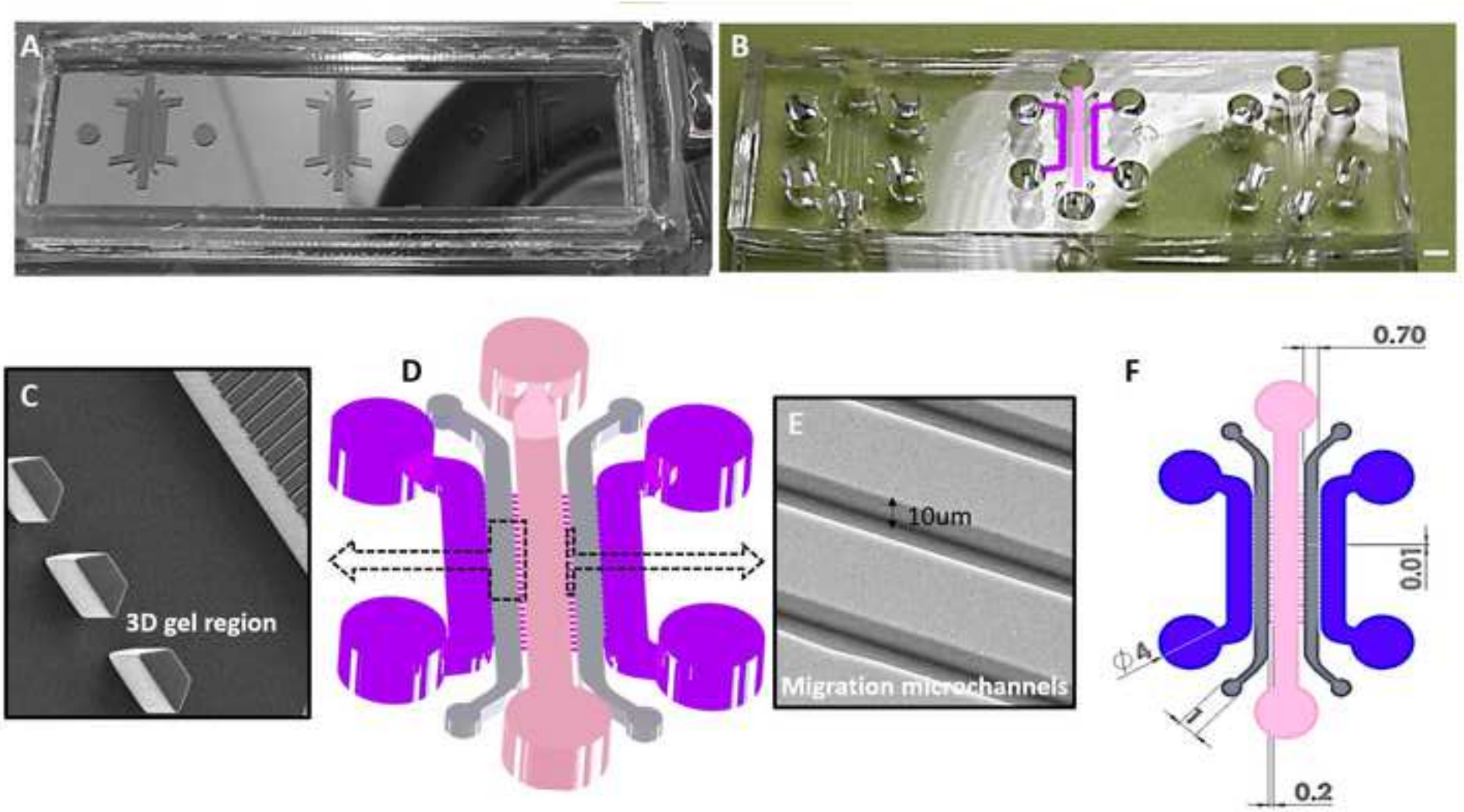

figure04.jpg

Figure

Click here to access/download;Figure;figure05_300dpi.tif

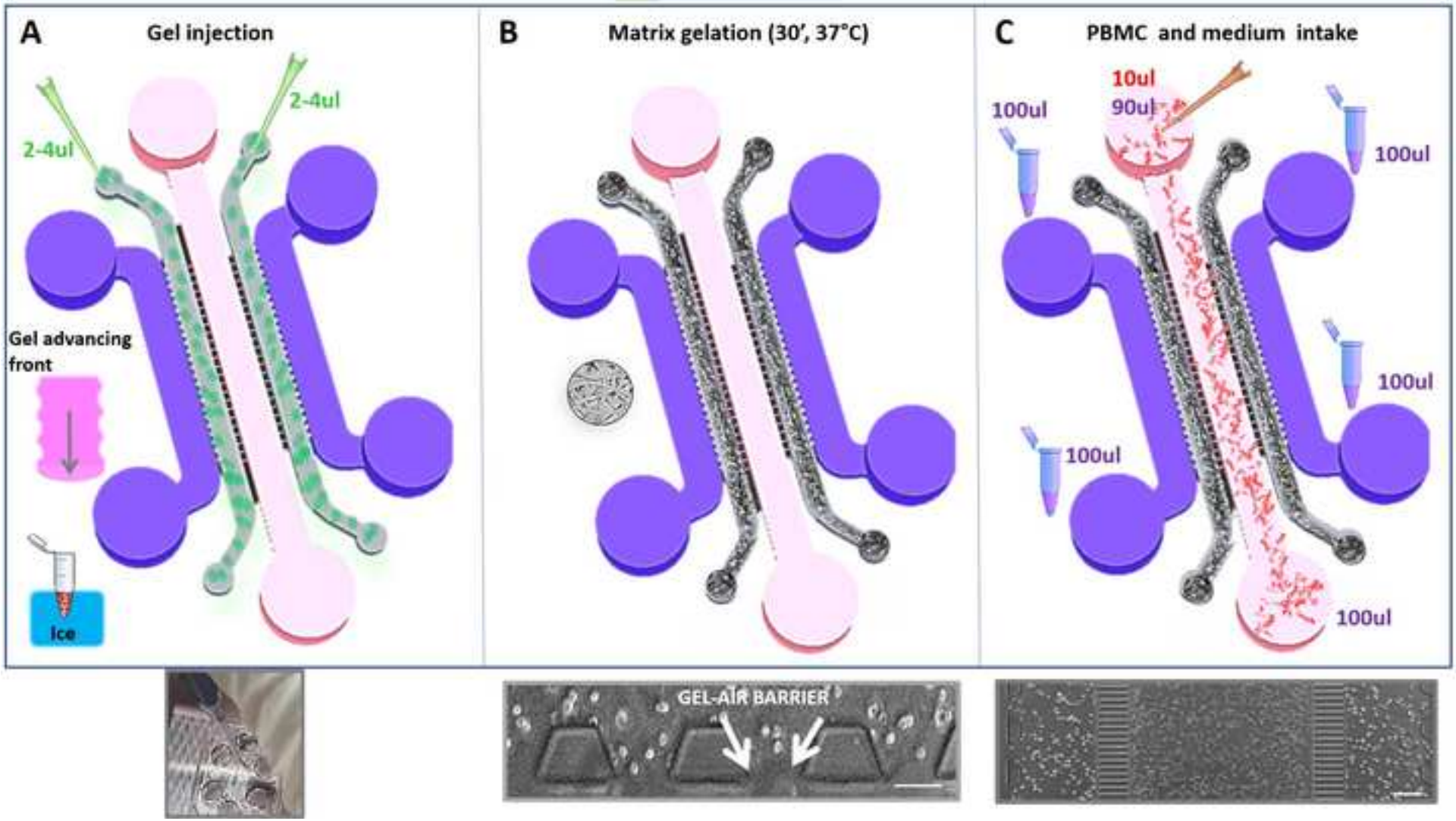

figure05.jpg

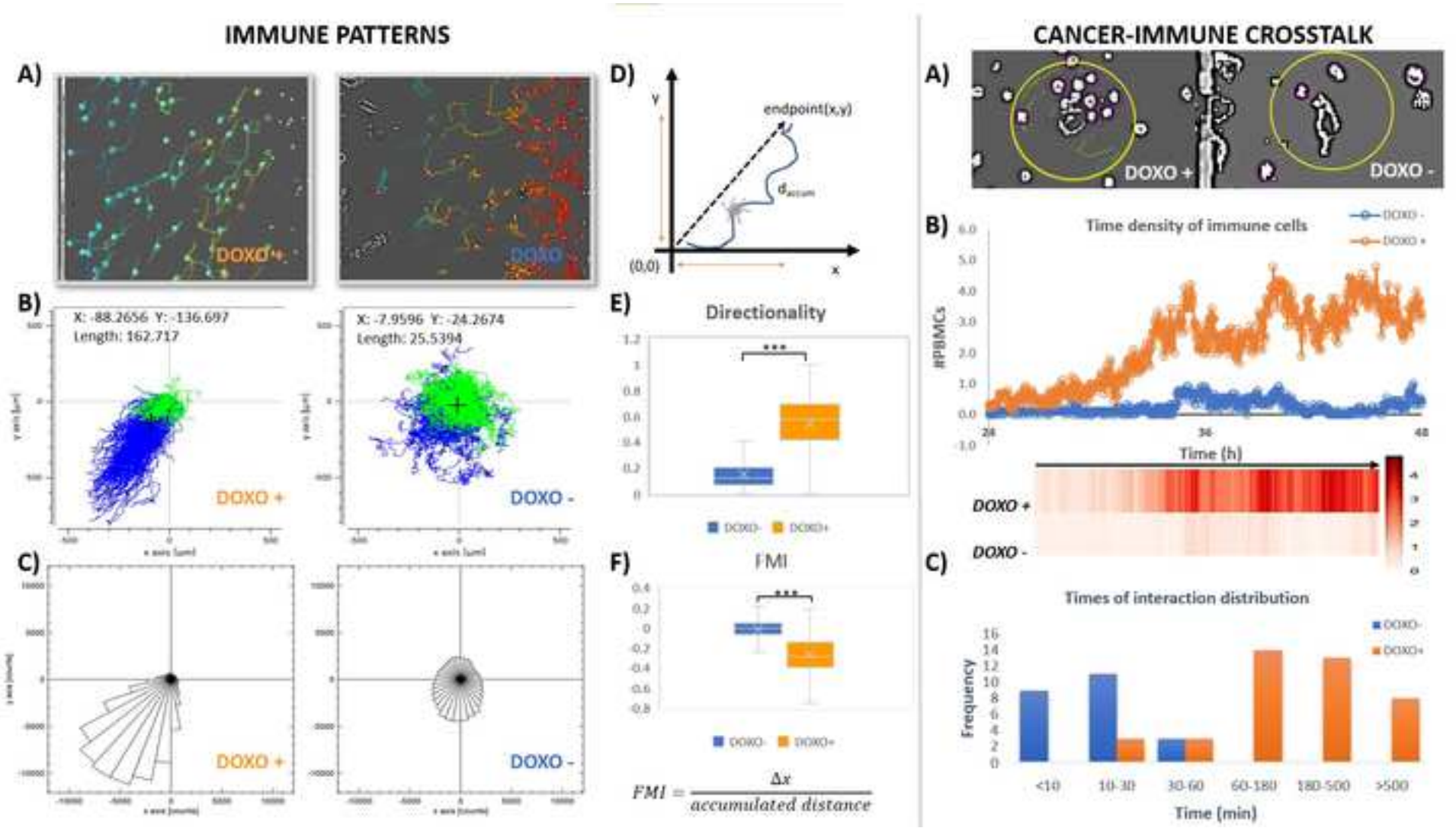

Figure

Click here to access/download;Figure;figure07_300dpi.tif

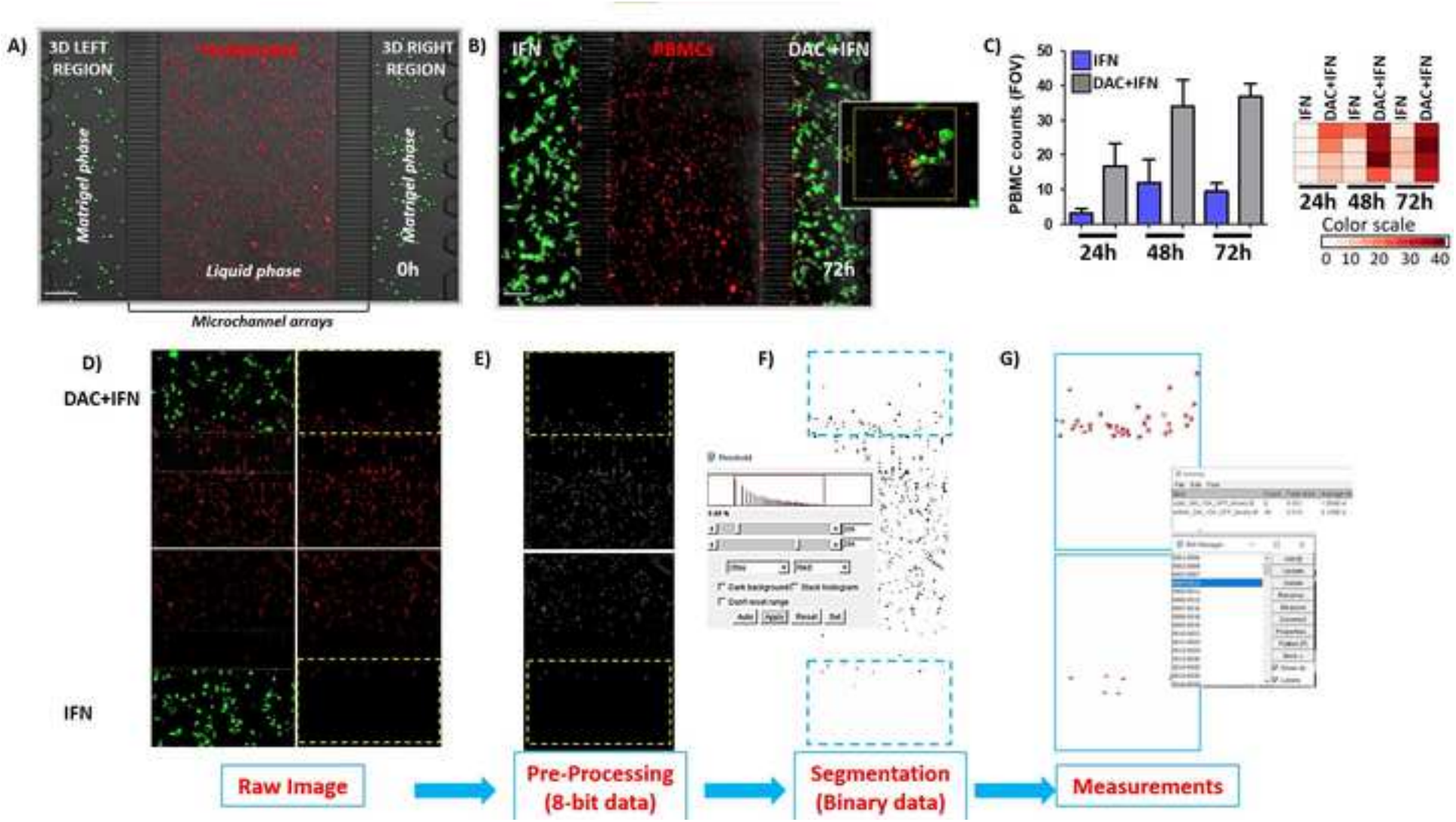

figure07.jpg

Video or Animated Figure

Click here to access/download

Video or Animated Figure

Timelapse_PBSvsDOXO_PBMCs_WT_0-24h_01.mov

Name of Material/ Equipment	Company
Cell culture materials	
50 mL tubes	Corning-Sigma Aldrich, St. Louis, MO
5-aza-2'-deoxycytidine DAC	Millipore-Sigma; St. Louis, MO
6-well plates	Corning-Sigma Aldrich, St. Louis, MO
75 cm2 cell culture treated flask	Corning, New York, NY
A365M	American Type Culture Collection (ATCC), Manassas, VA
Doxorubicin hydrochloride	Millipore-Sigma; St. Louis, MO
Dulbecco's Modified Eagle Medium DMEM	EuroClone Spa, Milan, Italy
Dulbecco's Phosphate Buffer Saline w/o Calcium w/o Magnesium	EuroClone Spa, Milan, Italy
Fetal Bovine Serum	EuroClone Spa, Milan, Italy
Ficoll	GE-Heathcare
hemocytometer	Neubauer
Heparinized vials	Thermo Fisher Scientific Inc., Waltham, MA
interferon alpha-2b	Millipore-Sigma; St. Louis, MO
L-Glutamine 100X	EuroClone Spa, Milan, Italy
Liquid nitrogen	
Lympholyte cell separation media	Cedarlane Labs, Burlington, Canada
Lymphoprep	Axis-Shield PoC AS, Oslo, Norway
Matrigel	Corning, New York, NY
MDA-MB-231	American Type Culture Collection (ATCC), Manassas, VA
Penicillin/ Streptomycin 100X	EuroClone Spa, Milan, Italy
Pipet aid	Drummond Scientific Co., Broomall, PA
PKH26 Red Fluorescent cell linker	Millipore-Sigma; St. Louis, MO
PKH67 Green fluorescent cell linker	Millipore-Sigma; St. Louis, MO
RPMI-1640	EuroClone Spa, Milan, Italy
serological pipettes (2 mL, 5 mL, 10 mL, 25 mL, 50 mL)	Corning- Millipore-Sigma; St. Louis, MO
sterile tips (1-10 µL, 10-20 µL, 20-200 µL, 1000 µL)	EuroClone Spa, Milan, Italy
Timer	

Trypan Blue solution	Thermo Fisher Scientific Inc., Waltham, MA
Trypsin	EuroClone Spa, Milan, Italy

Cell culture equipment

EVOS-FL fluorescence microscope	Thermo Fisher Scientific Inc., Waltham, MA
Humified cell culture incubator	Thermo Fisher Scientific Inc., Waltham, MA
Juli Microscope	Nanoentek
Laboratory refrigerator (4 °C)	FDM
Laboratory Safety Cabinet (Class II)	Steril VBH 72 MP
Optical microscope	Zeiss
Refrigerable centrifuge	Beckman Coulter
Thermostatic bath	

Microfabrication materials

3-Aminopropyl)triethoxysilane (Aptes)	Sigma Aldrich
Chromium quartz masks / 4"x4", HRC / No AZ	MB W&A, Germany
Glass coverslip, D 263 M Schott glass, (170 ± 5 µm)	Ibidi, Germany
Hydrogen Peroxide solution 30%	Carlo Erba Reagents
Methyl isobutyl ketone	Carlo Erba Reagents
Microscope Glass Slides (Pack of 50 slides) 76.2 mm x 25.4 mm	Sail Brand
Miltex Biopsy Punch with Plunger, ID 1.0mm	Tedpella
PMMA 950 kDa	Allresist,Germany
Polymer untreated coverslips	Ibidi, Germany
Prime CZ-Si Wafer, 4”, (100), Boron Doped	Gambetti Xenologia Srl, Italy
Propan-2-ol	Carlo Erba Reagents
Propylene glycol monomethyl ether acetate (PGMEA)	Sigma Aldrich
SU-8 3005	Micro resist technology,Germany
SU-8 3050	Micro resist technology,Germany
Suite of Biopunch, ID 4.0 mm, 6.0 mm, 8.0 mm	Tedpella
Sulfuric acid 96%	Carlo Erba Reagents
SYLGARD 184 Silicone Elastomer Kit	Dowsil, Dow Corning

Trimethylchlorosilane (TMCS)	Sigma Aldrich
Microfabrication equipment	
100 kV e-beam litography	Raith-Vistec EBPG 5HR
hotplate	
Optical litography system	EV-420 double-face contact mask-aligner
Reactive Ion Etching system	Oxford plasmalab 80 plus system
Vacuum dessicator	

Catalog Number	Comments/Description
CLS430828	centrifuge tubes
A3656	DNA-hypomethylating agent
CLS3506	culture dishes
430641U	culture flasks
CVCL_B222	human melanoma cell line
D1515	anthracycline antibiotic
ECM0728L	Culture medium for SK-MEL-28 cells
ECB4004L	saline buffer solution
ECS0180L	ancillary for cell culture
17-1440-02	separation of mononuclear cells from human blood.
	Cell counter
	Vials for venous blood collection
SRP4595	recombinant human cytokine
ECB3000D	ancillary for cell culture
	Separation of lymphocytes by density gradient centrifugation
354230	growth factor reduced basement membrane matrix
HTB-26	human breast cancer cell line
ECB3001D	ancillary for cell culture
4-000-201	Liquid handling
PKH26GL	red fluorescent cell dye
PKH67GL	green fluorescent cell dye
ECM2001L	Culture medium for MDA-MB-231 cells
CLS4486; CLS4487; CLS4488; CLS4489; CLS4490	Liquid handling
ECTD00010; ECTD00020; ECTD00200; ECTD01005	tips for micropipette

15250061	cell stain to assess cell viability
ECM0920D	dissociation reagent for adherent cells
	Fluorescent microscope for living cells
311 Forma Direct Heat COIncubator; TC 230	Incubation of cell cultures at 37 °C, 5% CO_2
	Laminar flow hood
A3648	silanizing agent for bonding PDMS to plastic coverslip
	optical masks for photolithography
10812	
412081	reagents for piranha solution
461945	PMMA e-beam resist developer
7101	substrates for bonding chips
	dermal biopsy punches for chip reservoirs
AR-P. 679.04	Positive electronic resists for patterning optical masks
10813	substrates for bonding chips
30255	
415238	
484431-4L	SU-8 resists developer
C1.02.003-0001	Negative Photoresists
C1.02.003-0005	Negative Photoresists
15111-40, 15111-60, 15111-80	dermal biopsy punches for chip reservoirs
410381	reagents for piranha solution
11-3184-01	Silicone Elastomer (PDMS)

92360-100ML	silanizing agent for SU-8 patterned masters

We would like to thank the reviewers and the editor for their in-depth reading of our paper and for comments that allowed us to identify unclear aspects of the paper, to go deeper in some details of the illustrated workflow, and highlight critical aspects of the protocols, yet clarifying the potentialities of the approach. After significant revision, we believe that the manuscript has been improved both in completeness and clarity. You will find the answers to your comments in this point-by-point response, and major changes highlighted (in red) in the text of the paper.

Reply to the editorial comments:

Changes to be made by the Author(s):

1. Please take this opportunity to thoroughly proofread the manuscript to ensure that there are no spelling or grammar issues.

The whole manuscript has been proofread; we think that the overall language quality has been improved.

2. Unfortunately, there are sections of the manuscript that show overlap with previously published work. Please revise the following lines: 806-814, 833-839

All the sections have been revised, and lines 806-814, 833-839 rewritten.

3. How is the supplemental video to be used? Please provide a legend for it in the manuscript.

A legend for the supplemental video showing exemplary co-cultures of tumor cells and PBMCs in the 2D chip setting has been added. The rationale is to use it for the preparation of the video of the protocol in Jove.

4. Please ensure that all text in the protocol section is written in the imperative tense as if telling someone how to do the technique (e.g., “Do this,” “Ensure that,” etc.). The actions should be described in the imperative tense in complete sentences wherever possible. Avoid usage of phrases such as “could be,” “should be,” and “would be” throughout the Protocol.

All sections of the protocol now include only action items.

5. The Protocol should contain only action items that direct the reader to do something. Please move the discussion about the protocol to the Discussion.

Additional text is included now as a note or transferred to the Discussion.

6. Please highlight up to 3 pages of the Protocol (including headings and spacing) that identifies the essential steps of the protocol for the video, i.e., the steps that should be visualized to tell the most cohesive story of the Protocol. Remember that non-highlighted Protocol steps will remain in the manuscript, and therefore will still be available to the reader.

We have provided the requested additional pages that illustrate the essential steps of the protocol for the video.

7. Please ensure that the highlighted steps form a cohesive narrative with a logical flow from one highlighted step to the next. Please highlight complete sentences (not parts of sentences). Please ensure that the highlighted part of the step includes at least one action that is written in imperative

As suggested by reviewers' comments we have added a supplementary file to describe steps of fabrication, from the realization of optical masks, and masters for soft lithography to the production of final PDMS chips.

Reviewers' comments:

Please note that page and line numbers mentioned hereafter refer to our revised manuscript and not to the original paper. The changed and added texts are shown in red.

Reviewer #1:

Manuscript Summary:

The authors describe a novel organ-on-chip approach to investigate the interaction between tumor and immune cells in in vitro tumor microenvironment. They show two different devices to create 2D or 3D co-cultures in order to study the immune response toward tumor. It is well written and data are clearly present.

Minor Concerns:

1. The authors point out in part 1 relating to the 2D device that "fresh media should be added every 3 days due to evaporation". This note should also be added in Part 2 related on 3D devices, indeed the evaporation could lead to variations in the volume of medium in the chip.

Authors' response: We agree with the reviewer, evaporation indeed represents one of the critical issues to be monitored in organs on chip experiments. As suggested, we have added a note in section 2, step 1.12 (lines 507-508).

2. The authors should discuss if it is possible to analyse in the chip: the phenotype, the functional status of the migrated immune cells and the chemokines released in order to evaluate the mechanism of tumor and immune cell interaction.

Authors' response: We thank the referee to go in depth with this point of discussion. There are indeed several methods to characterize cellular populations in cocultures.

To characterize their dynamic behavior in living conditions, specific immune cell sub-populations can be isolated by means of immunomagnetic bead selection, stained with fluorescent cell trackers or by gene reporters, re-mixed with the unlabeled remaining fraction, and thus confronted with target cancer cells, as reported in on-chip experiments, described in Vacchelli et al. Science 2015 and in Racioppi et al., Nat Comm, 2019. A note has been provided in section 1 (paragraph "Plating the cells in 2D chips", page 4, lines 208-2012).

The described models are compatible both with live/dead-cell analysis and dynamic multiplex cytokine secretion profiling from conditioned media. For chemokine analyses, up to 100-250 µl aliquots of supernatants may be accessible by collected media from the two reservoirs of each compartment for 2D and 3D chips. Classical ELISA and Luminex cytokine profiling assay require about 50µl volumes. We have inserted references of studies of other labs performing cytokine profiling on organs-on chip models. We have inserted a note in section 1, step 2.7, page 5 , lines 242-247.

Staining for nuclear and active caspases, by using commercial kits for Live/dead assays (e.g Incucyte reagents), can be implemented in order to assess proliferation/apoptotic death events as we performed in a previous study (reported in Nyugen et al., Cell Reports 2018). We have inserted a note in section 2, page 9, lines 445-447.

Additionally, classical methods of immunofluorescence and confocal high-resolution imaging/analysis can be applied to on-chip operations. Standard immunofluorescence staining procedure involves cell fixation, permeabilization, blocking, antibody binding, with washing steps in between. Immune cells infiltrated in 3D gels regions with embedded cancer microenvironments can be fixed at desired endpoints and stained for expression markers of activation/exhaustion /maturation (e.g, for CD8 cells, monitoring of CD69, CD95). In Parlato et al., we have evaluated phagocytosis of SW620 apoptotic cells by confocal microscopy. IFN-DCs were stained by inserting on-chip anti-human HLA-DR-FITC Ab aliquots. We have inserted a note in section 2 page 11 , lines 513-521.

Reviewer #2:

Manuscript Summary:

In-vitro models that recapture the tumor microenvironment in their entirety or include critical components of the tumor including the stroma, immune and non-immune cells are the need of the hour. While it's important to develop such models, it's even more essential to demonstrate its functionality and validity to the scientific community. Detailed protocol articles like the current one under review make it easier for fellow researchers to reproduce and adapt the methodology into their own projects and laboratories. The article is written very well and clear instructions are provided for each step with figures.

Major Concerns:

No major concerns

Minor Concerns:

None

Authors' response: We thank the referee for appreciating our work.

Reviewer #3:

The authors developed a microfluidic technique that allows the coculture of cancer cells with immune cells to capture their interaction both in 2D and in 3D. The data were quantified following a Fiji-based algorithm to visualize cellular functions. A protocol for the technique is clearly explained. The article should be published after the following comments are addressed:

1. Line 156 should read 1.1, not 4.1.

Authors' response: The numbers in the list are now correct (in the revised text, page 4, line 167).

2. In part 1.25, the authors may want to indicate the media that was used (or that it is the same media used for the cancer cells).

Authors' response: We now specify in the text (section 1, step 1.25, page 4, line 203) that the media is the same used for cancer cells.

3. Is there a technique the authors employ to inhibit the formation of bubbles within the microfluidic device?

Authors' response: In the described protocols, 2D and 3D chips are realized in Polydimethylsiloxane (PDMS). The surface of PDMS is naturally hydrophobic. To modify wettability, oxygen plasma activation is the standard method used for both its switching to a hydrophilic state and the irreversible PDMS-substrate (i.e., glass or plastic slides) bonding. Typically, our process involves high gas pressures and low RF (radiofrequency) power, in a reactive ion etcher (RIE) If needed, before biological experiments, we perform an additional O_2 plasma treatment of stored assembled, previously sealed, chips to restore the desired hydrophilicity degree. This is normally sufficient to avoid bubble formation during culture medium loading. We have added an additional step (section 1, step 2.1, page 4, lines 214-219) in the protocol relative to 2D chips in the manuscript. Moreover, we have provided details for surface modification of both 2D and 3D chips in the supplementary file dedicated to microfabrication steps (step 7).

4. In part 2.2, the authors specified that functionalizations of the surface can be made. It may be useful to provide examples and how to perform such functionalizations.

Authors' response: Various polymer and extracellular matrices (e.g., Matrigel, Fibronectin, Collagen) coating solutions can be used for different cell types under study. Standard functionalization procedures include loading surface coating solution in all reservoirs for a certain time, followed by some washes in with deionized water, PBS or medium. We included in the text references of previously published protocols to accomplish functionalization steps in section 1, step 2.4, lines 229-231.

5. What are the proper dimensions for the micropillars to ensure a balance between surface tension and capillary forces?

Authors' response: For the 3D chip layout, we designed two arrays of about 20-30 isosceles trapezoidal pillars with a spacing of 100 microns. Post barriers were tested empirically based on previous work of CP. Huang et al., Lab on Chip 2009. We have reported dimensions in a note, in section 2 (page,9 line 432-434) and added proper references of previous studies relative to modeling the filling process of gels in microchambers in presence of micropillars.

6. Line 405 should have the abbreviations spelled out.

Authors' response: We have transferred this note in lines and now the drugs abbreviations have been spelled out firstly in step 1.2, lines 462-463.

7. In line 459, the authors mention that adjustments should be made if the distribution of cells is not optimal; would these adjustments need to be made on a new chip? A clarification would be useful.

Authors' response: In the paper we now clearly state to use always new chips (steps 1.10, lines 501-503). We also suggest considering having a 10%-20% more spare chips respect to the number of conditions to be monitored.

8. The paragraph starting in line 750 is unclear.

Authors' response: We changed the sentence in the Discussion, page 18, line 823.

9. The different improvements to the system broken up per section is a nice touch to the manuscript.

Authors' response: We thank the reviewer for appreciating the configuration of the paper.

10. For publication, ensure the red underlines under the words in the figure are not present.

Authors' response: We corrected the problem.

11. In Figure 2C, why does the mean intensity increase from left to right (the color changes from blue to red)? Is this an artifact of the microscope?

Authors' response: We thank the reviewer for detecting this error. The old panel (label "mean intensity" in the drop menu) has been replaced with the correct screenshot (filter label in the drop-menu: X) of Trackmate menu in the revised Fig.2 The spots in the image shown in the Fig.2C, highlighted in the intermediate chamber of 2D chip are color-coded, depending on their position along X (in this example, immune cells, surrounded by blue circles are nearby the microchannels entrance). We have now specified in the caption of Fig.2.

12. The caption for Figure 3E does not include D nor E. Please include a sentence on each to clarify what is being shown.

Authors' response: We have corrected captions in D and E, wrongly indicated in the previous text by F and G.

13. There are various typographical errors throughout the manuscript that need to be fixed.

Authors' response: We have corrected various typographical errors and improved the revised manuscript. We would like to apologize for some of these lapses.

Reviewer #4:

Manuscript Summary:

This manuscript contains detailed protocols for tumor on-a-chip experiments. The authors are pioneers and experts in the field. These protocols will be very useful for other laboratories.

Major Concerns:

None

Minor Concerns:

1) Page 2, lines 105-106: A reference is needed after "This allowed us to characterize immune responses to cancer cells treated or not with immunogenic cell death inducers."

Authors' response: We introduced the associated reference in the Introduction, line 106.

2) Page 3, line 146. What do the numbers in "500x12x10 μm3" stand for? Please specify.

Authors' response: The text now includes specifications about size units in page 3, line 155.

3) In the protocols, technical details about chip design and construction should be provided so that other laboratories can produce or order identical chips.

Authors' response: Since chip fabrication protocol is similar to already published protocols in jove, we added the necessary references and the technical details to fabricate both 2D and 3D chips (from realization of photomasks, and SU-8 patterned masters to final assembled chips) a supplementary material.

4) Page 3, lines 146-147: "intermediate channel". Do the authors mean "intermediate chamber" instead?

Authors' response: We replaced the text as follow "The intermediate chamber forms two closed dead-end compartments which block floating immune cells overflowing into the tumor site when initially loaded" (page 3, line 156)

5) Catalog numbers should be provided for all reagents used in the protocols.

Authors' response: Now all catalog numbers of reagents/materials appear correctly in the revised version of the table "Jove Materials".

6) "IFN" is a confusing abbreviation because there are many types of interferons with different properties. The authors should specific with a Greek letter throughout the manuscript which exact interferon they refer to (alpha, beta, gamma, etc).

Authors' response: We modified the text to clarify the acronym's usage as follows: 'Where indicated, add 5-aza-2'-deoxycytidine (DAC; 2.5 μM), **referred to as DAC**, and/or IFN-α2b, r**eferred to as** IFN, at the proper doses''.

The use of IFN-alpha is indicated in section 2, page 10, step.1.2, line 462.

7) Page 13, line 597: "The results, strongly indicated" should be corrected to "The results indicated".

Authors' response: We have modified the sentence as suggested (page 14, line 629).

8) Page 13, line 604: negletible. Negligible, I suppose?

Authors' response: We revised the whole paper to correct this and (hopefully) all other misspellings.

9) Page 17, line 756. The authors state that "the choice of the culturing matrix is fundamental" without being more specific. Which culturing matrix and chip material would the authors currently recommend for tumor on-a-chip experiments?

Authors' response: We thank the reviewer for pointing out this point that is relevant in the definition of the experimental protocol. We added the necessary information and references in the text (page 10, step 1.1, line 457-459). We clarified that in the presented 3D model we did use Matrigel due to its ability to promote cell growth and self-organization, but in other models we successfully used collagen I. This is a rapidly evolving field, and an increasing number of hydrogels is being designed, produced and tested for specific models in organ on chip and organoid environment.

As detailed also in microfabrication section (supplementary file), the material used for the chip is PDMS, widely used as standard material with soft-lithography protocols and for its compatibility with cell culture.

10) Page 18, lines 795-803. The authors state that "immune cells are could be heavily perturbed by time-consuming, complex and expensive staining procedures" and apparently recommend "the usage of label free observation of the immune system". It is a surprising recommendation which would imply a significant limitation of this technique. If many different cell types are added to a chip recreate in vitro a tumor microenvironment, it will be essential to be able to identify the different cell types during an experiment. Although labeling procedures have limitations such as toxicity, they are widely used for in vitro live imaging experiments. It is hard to believe that cell labeling could not be used on-a-chip. This important technical point needs clarification.

Authors' response: We thank the reviewer for the possibility to better explain this point. Fluorescence labeling, due to its high specificity, undoubtedly represents a gold standard method to identify different cell populations in co-culture conditions, and in OOC models this approach is commonly used as a reference. However, when dealing with immune cells, extra care must be taken to avoid perturbing effects induced by fluorophore molecules and illumination routines, that can deeply affect cell behavior and state. Moreover, the maximum number of simultaneous fluorescent colorations available, could constitute a limiting factor in the observation of multi cell-type contexts exploited in OOC experiments. In this context an increasing number of researches are dealing on classification and recognition of different cell type/activity using Artificial Intelligence based image analysis and/or different optical approaches.

In the revised Discussion section, named "Beyond Fluorescence Imaging" (page 19, lines 863-887) we list some emerging possibilities, which we think will be fruitfully included in OOC workflow in the next future to complement the use of fluorescence imaging. In particular we refer to both directions: the exploitation of new imaging approaches (e.g., hyperspectral, holographic), and the adoption of machine learning methods, such as ones providing strategies (trained by fluorescence images datasets), to perform the so called ' *'in silico* labeling'', applied to predict fluorescent markers from bright-field images, promising a good classification accuracy without actual labelling of cells.

.

11) Page 18, line 821. What exactly do the authors mean by "omics". Please specify.

Authors' response: We better specified this point in the text by referring to single-cell omics techniques in page 20, lines 916.

Reviewer #5:

Manuscript Summary:

The authors describe a microfluidic platform for co-culture of cancer cells with stromal cells and show immune targeting in response to various treatments. The authors also describe their image processing methods.

Major Concerns:

5.1 The authors highlight the use of fluorescence microscopy in the tracking of cells in the microfluidic platform, yet the video they provide is brightfield only. Fluorescence time-lapse microscopy is warranted and would be helpful to include in order to visually differentiate between the cancer cells and the immune cells in the platform.

A viability marker would be useful to show the cancer cell death.

Authors' response:

We thank the reviewer for providing opportunity to clarify better the rationale of having two different sections. We have now revised the abstract to introduce more clearly this aspect (lines 38-49). In the paper we provide protocols relative to two distinct microfluidic assays, for assembling respectively 2D (Fig.1A), and 3D (Fig.4A) co-cultures of tumor and immune cells. In 2D setting we performed visible light time-lapse movies of unlabeled co-cultures. In the 3D setting we monitored immune infiltration towards tumor cells cultivated in 3D regions, acquiring only fluorescence snapshots at specific endpoints (thus not videos).

and We detailed in Discussion paragraph (page 19, lines 863-887), advantages, limitations, and challenges of fluorescence- based methods in OOC imaging strategies, indicating some developments in label free techniques that will match fruitfully with multi cell-type contexts such OOC models and we inserted explicit references to previous work from our and other groups

Concerning the theme of compatibility with commercial kits for Live/dead assays for live-cell imaging, we explicitly added a note in the protocol section 2 (page 9, lines 445-448), and linked references to other studies from our group describing the possibility to perform on-chip staining for nuclear and active caspases to assess proliferation/apoptotic death events .

5.2 In the video, it is not clear what the difference between the two 'PBMC WT' panels is, and this is also not described in the text.

Authors' response: We inserted the missing caption for the supplementary movie (0-24h interval) (page 17, line 764-770]. In the caption and in Results (Fig.6, lines 613-651) is now clearly described the difference among the panels: PBMCs extracted from healthy donors (WT, wild type), were plated with human MDA-MB-231 breast cancer cells, non-treated or exposed to DOX (an immunogenic cell death inducer, ICD). In the second case, PBMC's migration appears clearly, while in the non-treated case they are poorly or not attracted by proliferating untreated cancer cells (left panel movie).

5.3 I would suggest for the video, to include a walk-through of your image processing software. There are many steps and options, so to have that portion visualized for the user would be exceptionally helpful.

Authors' response: We thank the referee for the valuable suggestion for the making of the video.

5.4 Chip fabrication steps are not included here but needed in order to carry out experiments. This also has implications for imaging - what is the focal length of the chip bottom? Are the devices arrayed for high throughput experiments? How many devices can you feasibly load and run at a time? This also has a bearing on the feasibility for AI integration.

Authors' response: As discussed in the response to reviewer 4 point 3, we did include details of chip fabrication, from the realization of optical masks, and masters for soft lithography to the production of final PDMS chips as supplementary material.

For the throughput point, typically 3 chips are arranged on a single microscope slide (Fig.1A for 2D chip, 4A for 3D chip). So, it is possible to monitor up to 12 chips, using holders allocating 4 slides by high-content microscopy (e.g. Operetta imaging systems, Molecular devices, ImageXpress systems) to increase batches of experimental conditions. Chips can be easily mounted on slides with thickness equal to 1mm or 170 microns (plastic or glass coverslips, 6-well optical multi-wells) for high-resolution confocal imaging. We have inserted in the revised manuscript a specific note in page 5, line 250-255 and discussed the throughput point in the paragraph Data Management of Discussion (lines 840-854).

Additionally, as strategy to keep compatibility with automated acquisition routines of high-content microscopes, we have introduced detailed steps in the supplementary file "microfabrication protocol" (page 3, step 6 of the supp file). Typically, we realize markers on glass or plastic slides (to which PDMS chips will be bonded) by laser cut systems. Markers are used to align slides, in a standardized way, with respect to PDMS chips. This aids to integrate chips in automated imaging settings.

5.5 The use of artificial intelligence is mentioned, however specific examples of how AI can be leveraged in the proposed context are missing. AI requires large datasets, and it is not clear from the article how the technology will either integrate or generate large datasets to leverage AI algorithms.

Please describe with concrete examples how you plan to move forward with AI in the current context, since this is only peripherally alluded to in the text.

Authors' response: We agree with the reviewer that this point was poorly tackled in the previous version of the paper. We expanded the discussion and added, where relevant, a description of the potential contributions of AI schemes in OOC data analysis:

1) "*in silico* labeling'' to predict fluorescent markers from bright-field images. This can also be suitable to reduce photodamage for sensitive samples, to save time in acquisition and fluorescence channels for other markers, particularly useful in contexts such as multi-cell type OOC models. (page 20, lines 881-887).

2) from managing critical imaging acquisition parameters to improving image segmentation steps, such as implemented in microscopy software packages (page 20, lines 904-906).

3) Recognition of common cellular patterns (e.g., motion styles) in order to characterize the biological response with respect to microenvironmental factors. Such an example of potentiality of this point, we reported the study, described in Comes *et al., Scientific Reports,2020*, regarding the classification of immune patterns, extracted from time-lapse data of 3D co-cultures of cancer cells and PBMCs in our microdevices (page 20, lines 910-913).

5.6 It is not clear to me why there are two sections and two seemingly distinct script programs that appear to be doing similar processes. I would consider integrating '4 Data analysis: Semi-automatic extraction of immune tracks by Trackmate' and '2 Automated Counting of recruited PBMCs in single channel fluorescent images in ImageJ' into a single package. It states that Trackmate can process fluorescent images, so why the separate section for fluorescent images? This is not clear to me from the text. Please plainly state the difference if there is one or merge the two sections into one section on image processing toward the end of the text if possible.

Authors' response: We improved the paper to clarify the need for the two different sections stressing the different experimental approaches and data analysis of the two different scenarios as additive or complementary modules of the OOC approach in the onco-immunology field (in the Abstract, and in the Introduction lines 93-132).

In the section 1 we describe a system where adherent cells (tumor cells) and floating cells (immune cells) interact to recapitulate immune response to cancer immunogenic inducers and were imaged by time-lapse bright-field microscopy with short time interval (2min) up to 48h. In this case we present the semi-automatic analysis pipeline based on Trackmate to build tracks of unlabeled immune cells, and to process motility and interaction patterns.

In the section 2 the contribution describes the use of a novel chip to recreate tumor-immune microenvironments in 3D gels in a ''competition layout". Differential migration of immune cells towards two compartments hosting tumoral cells that have undergone different treatments can be monitored and quantified. For the image analysis point of view, we acquired fluorescence snapshots of stained PBMCs in some ROIs (not time-lapse videos with short time interval) at 0h, 24h, 48h,72h. We extract counts (not tracks) of labeled PBMCs infiltrated in 3D matrices with embedded tumor cells. Therefore, we described segmentation steps for fluorescence images and subsequent counting by Analyze plugin in Image J. Of course, in case of fluorescent time-lapse series, Trackmate procedure (as in the section1) can be applied.

Minor Concerns:

Please cite protocols that have already been extensively published (e.g. PBMC isolation).

Authors' response: We have introduced reference to protocols in lines

Please consider referencing the work of Christopher Hughes, Don Ingber and Roger Kamm.

Authors' response: We have introduced a reference for the vascularized tumor platform developed by C.Hughes (line 90) and added several citations to D.Ingber (ref 13,14,86) and R.Kamm works in the revised manuscript (line 90, ref. 19-21, ref. 61).

There are many grammatical errors and the list below is not a comprehensive list of the errors found in the manuscript.

Authors' response: We would like to apologize for the several errors, and we revised extensively the manuscript to improve clarity and correctness.

99 - not clear what is intended in this sentence, as it states 'a microfluidic device thought to'. Do you think it does this or is this something you've shown? Statement doesn't read as scientific.

Authors' response: We replaced by term designed (page 2, line 99).

107 - what is meant by 'long-term' here? How long can these be cultured/imaged?

Authors' response: We modified by timeseries images. In the described experiments, we monitored co-cultures in microfluidic devices (2D or 3D settings) up to 48-72 hours.

114 - Please define what A375M and A375P are and what is the difference.

Authors' response: A375M are a metastatic melanoma cell line while A375P are a primary melanoma cell line. We have explained the difference in the revised version of the Introduction (page 2, lines 117-120).

116-118 - Have you shown cells derived from these sources to work in this platform? If so, please provide references.

Authors' response: The section 2 of the protocol (3D setting) involves the use of human A365M melanoma cell lines in Matrigel exposed to combinations of therapeutic agents, and primary peripheral blood mononuclear cells (PBMCs) from healthy donors. Despite the A375P primary cell line, A375M was chosen to evaluate their metastatic capability in presence of immune cells. We have provided the associated reference in page 2, line 120. As highlighted in the introduction, the developed models can be fully compliant with different cell sources (i.e., murine and human immortalized or primary cell lines, organoids, xenografts). We inserted references (lines 101-102, and lines 124-132) of several published works of our lab in the introduction.

120 - Which ADCC is being tested?

Authors' response: In our previous study, (reported in Nguyen et al. Cell Reports 20x 18) we have reconstituted ex vivo a human tumor ecosystem (HER2+ breast cancer) in the presence of the drug trastuzumab (Herceptin), a targeted antibody therapy directed against the HER2 receptor. We demonstrated that the presence of trastuzumab, in addition to inhibiting cancer cell proliferation and stimulating cancer cell death as expected, increased cancer-immune interactions and induced an anti-

tumoral ADCC immune response. We have changed the text to add more details (page 2, lines 125-126).

Authors' response: We have fixed the following errors, according to suggestions.

Methods 3.1 - stating the power should be left on while warming up the microscope is not needed (goes without saying)

574 - response to therapy needs a period after

598 - should be 'exposed to DOXO or non-treated'

620 - close parentheses

731 - should be stress, not stress out

737 - on chip should be on-chip

830 - this is not a complete sentence…

840 - it is, not is

841 - requires, not is required

Supplementary file
Microfabrication protocol of PDMS chips

Polydimethylsiloxane (PDMS, Sylgard 184 kit, Dowsil), microfluidic assays for 2D (Fig.1, PART1) and 3D (Fig.4B, PART2) layout have been manifactured by well-known soft-lithographic procedures, as described in detail previously, in a clean room facility or foundry, equipped with micro- and nanoscale instrumentations (e-beam lithography, photolithography and thin-film technology, nano-diagnostic tools). NOTE: In the absence of clean room services, there are different companies on the market to order patterned optical masks or masters for PDMS soft-lithography.
Steps can be summarized briefly in the points below:

1. **Fabrication of optical masks.** NOTE: For both 2D and 3D chips two photomasks have been patterned by transferring CAD drawings containing layers respectively of culture chambers and microchannels with alignment marks.
   1.1. Spin PMMA (AR-P. 679.04, Allresist, Germany) positive electronic resist on chromium photomasks (MB W&A, Germany) at 2000rpm for 60sec.
   1.2. Pre-bake on a hotplate at 170°C for 5 min.
   1.3. Expose by 100 kV e-beam lithography. NOTE: E-beam (Raith-Vistec EBPG 5HR system) settings are the following: 650µC/cm^2 resist dose and 90nA e-beam current.
   1.4. Develop in MIBK: IPA = 1:1 (Methyl isobutyl ketone: Propan-2-ol, Carlo Erba reagents) for 30-60sec and rinse in IPA
   1.5. Place optical mask in a RIE (Reactive Ion Etching) chamber to perform O_2 plasma etch for 30 sec.
   1.6. Remove remaining chromium film in Cr etching acid solution for 2 min.
2. **Fabrication of a microstructured epoxy resin mould, referred to, as ''master''**. NOTE: Both 2D and 3D layout are patterned using two different i-line (365 nm, EV-420 mask-aligner) optical lithography onto the SU-8 3000 series negative sensitive epoxy resins (micro resist technology GmbH, Germany).
   2.1. Spin SU-8 3005 at 1000 rpm for 60sec to reach a thickness of about 10 microns.
   2.2. Pre-bake at 95°C for3 min. Choose post-bake temperatures and time according to manifacture datasheet.
   2.3. Expose the wafer to UV light through optical mask (4-5sec, 12.9mW/cm^2, EV-420 double-face contact mask-aligner)
   2.4. Post-bake at 65°C for 1 min and at 95°C for 2 min.
   2.5. Develop in PGMEA solution (Propylene glycol monomethyl ether acetate, Sigma Aldrich) and rinse in IPA for 10min.
   2.6. Hard-bake the wafer at 150°C for 30min.
   2.7. Spin SU-8 3050 resin to expose cell culture chambers to reach a desired thickness (1000 rpm for 30sec for 2D 100µm-high culture chambers, depicted in Fig.1)
   2.8. Pre-bake the wafer according to datasheet.
   2.9. NOTE: For 3D chip layout (Fig.4), repeat steps 2.7 and 2.8 twice to obtain a thickness range of 250-260µm (first spinning step: 2000 rpm for 30sec, second spinning step: 1100 rpm for 30sec)
   2.10. Expose (17sec,12.9mW/cm^2, EV-420 double-face contact mask-aligner).
   2.11. Execute post-bake of the wafer according to datasheet.
   2.12. Develop in PGMEA solution and rinse in IPA.
   2.13. Hard-bake the wafer at 150°C for 1h.
3. **Dry silanization of SU-8 micro-structured master.**

3.1. Inside a ventilated chemical fume hood put few drops of the silanizing agent (Trimethylchlorosilane, TMCS, Sigma Aldrich) in a cup and place the O_2 plasma pre-treated master over it in a vacuum dessicator. Keep them under vacuum for different hours or overnight. Note: During this process, TMCS evaporates and forms a monolayer on master surfaces to prevent PDMS sticking on its features. Note: Wear safety glasses, gloves and face protection.

3.2. Place the wafer on the hotplate in the fume hood 150°C for 10-15 mins to cure and evaporate the excessive silane.

4. Casting of PDMS liquid solution on microstructured master

4.1. Degas prepolimer solution (10:1 v/v, monomer: curing agent mixing ratio) contained in a plastic cup in a vacuum dessicator for 30 minutes.

4.2. Remove any dust on the surface of the silicon wafer by using a nitrogen gun with a 0.45 µm filter.

4.3. Pour slowly PDMS solution over the master avoiding bubbles. Leave it under hood for 10 min at room temperature (RT) before baking.

4.4. Crosslink PDMS thermally for 1h 30 min at 110 °C on a hotplate. Let it cool.

4.5. Detach carefully from the silanized master with a surgical blade and tweezers. Cut polimerized pieces in desired sizes and punch reservoirs (access ports for introducing cells and media) by dermal biopsy tools (Tedpella). Use 6 mm biopsy punches to create wells in the 2D layout, while for 3D layout drill respectively 4mm (media reservoirs) and 1mm-sized holes (gel inlets) .

5. PDMS structure irreversible sealing to cell culture substrates by O_2 plasma treatment

5.1. PDMS-glass bonding.

5.1.1. Put PDMS chips (with patterned side facing up) along with the glass slides inside the RIE chamber (Oxford Plasmalab 80 plus system) at the following RIE settings: 20W (RF power), flux of 60 standard cc/minute, 800-mTorr (pressure), and 30 sec (time). Note: Optimize process parameters according to your plasma cleaner machine.

5.1.2. Bring into conformal contact the treated surfaces of the glass slide and PDMS device (channels side faced down) with each other at a clean bench. Check under an optical microscope the quality of bonding. Note: PDMS can be mounted on glass microscope slides (1mm thick), glass coverslips (170µm thick) and optical bottom 6-multiwells.

5.1.3. Bake on a hotplate at 80-90 °C for 2 h, to improve adhesion strength. To restore hydrophobicity in 3D culture chips, keep for more than 4 hours at same temperature. Store chips in sterile Petri dishes.

5.2. PDMS-plastic bonding.

5.2.1. Inside the fume hood, put few drops of the silanizing agent (3-Aminopropyl) triethoxysilane APTES, Sigma Aldrich) in a cup and place the O_2 plasma pre-treated polymer coverslips (Ibidi, Germany) over it in a vacuum dessicator. Keep them under vacuum for 1-2 hours.

5.2.2. Put into contact the silanized coverslip and pre-oxidized PDMS piece to assemble final device. Keep them in an oven or on a hotplate at 60-65°C for some hours.

6. **Compatibility with the automated acquisition software for high-content microscopy.** Note: Markers for aligning PDMS chips are defined by laser writing system (Trotec Speedy 100 laser cut with 35W maximum laser power).

6.1.1. **Holder Fabrication**. In order to load and write quickly the markers on your glass or plastic substrate, use the laser cutter to realize a holder for the microscope slides (12

in our example). Use as material to fabricate holder Plexiglas 5mm thick (50cm x 30cm foil). Note: Alternatively, use a 5mm thick Plexiglas foil for the holder's base and a 2mm thick foil for the holder's cover.

6.1.2. Cut two rectangles of 25cm x 21 cm (Laser Power 90%, speed 0,40cm/s, air ON, repetition rate 2000 Hz). Reduce power to 60% if you use 2mm thick plexiglass foils.

6.1.2.1. *Holder base (first rectangle)*, open 8 hexagonal holes to insert nuts 1cm apart from the borders on each side of the rectangle (size of the holes according to you nuts); You'll have to glue your nuts in the holes once you remove the Plexiglas from the laser cutting machine.

6.1.2.2. *Holder Cover (second rectangle)*, open six holes to insert bolts in the same positions on the rectangle that you used for the nuts' seating. Open 12 (6x6) rectangular windows of the same size of your microscope slides or coverslips (25mmx75mm in our case). Take care that these windows are placed at least at 2cm from the holder sides and 1cm distant from each other.

6.1.2.3. *Holder assembly:* Use 8 bolts to screw together the cover and the base

6.2. **Marker definition.**

6.2.1. Prepare the drawing for the markers to be engraved on the glass slides or coverslips considering their position in the holder you realized in step 6.1, so that they'll match the ones on the chips. Note: Realize suitable markers in your PDMS chip layout fabrication. In our case we defined two crosses 2mmx2mm in the empty space between chips on the SU-8 master to replicate on the final PDMS chip.

6.2.2. Insert your microscope slides in the rectangular seating in the holder.

6.2.3. Place the holder inside the laser cutting machine, taking care to have it aligned with the machine axis and set the origin of your cut on the upper left holder's corner.

6.2.4. Engrave the markers with parameter suitable for the material that you are using. Note: Settings for glass slides are: Power 60%, speed 15mm/s, repetition 500Hz; for plastic (COC or polycarbonate) slides are: Power 30%, speed 40mm/s, repetition 500Hz.

6.2.5. If some white powder is deposited during the process, clean it with a soft cloth and Isopropanol after having unmounted the substrates form the holder.

7. Hydrophilic surface functionalization of chips before starting biological experiments.

7.1. 2D layout (Fig 1A). To insert easily medium in culture chambers, oxygen plasma activate the assembled PDMS/culture substrates in the RIE chamber for 20-30 seconds.

7.2. 3D layout (Fig 2A). Optionally perform selective oxidation of central immune chamber ina plasma cleaner for 5-10 seconds. This will make the chamber hydrophilic preventing formation of bubbles during loading. Note: Cover gel ports and media channels reservoirs (e.g, by Kapton tape) to guarantee the correct gel matrix positioning by micropillars array and avoid leakage in adjacent chambers. Gel regions have to be kept hydrophobic.